Modification of gas permeability of thermoplastic elastomers

Zuzana Kalíková

Bachelor's thesis
2023

Tomas Bata University in Zlín
Faculty of Technology

Univerzita Tomáše Bati ve Zlíně
Fakulta technologická
Ústav inženýrství polymerů

Akademický rok: 2022/2023

ZADÁNÍ BAKALÁŘSKÉ PRÁCE

(projektu, uměleckého díla, uměleckého výkonu)

Jméno a příjmení:	**Zuzana Kalíková**
Osobní číslo:	**T20893**
Studijní program:	**B0711A130009 Materiály a technologie**
Specializace:	**Polymerní materiály a technologie**
Forma studia:	**Prezenční**
Téma práce:	**Modification of Gas Permeabiity of Thermoplastic Elastomers**

Zásady pro vypracování

Student will describein bachelor work principles of gas permeability through thin layers of solid materials, further description of diferences between different polymers will be introduced ad possibiilites of gas permeability through elastomers with special focus to thermoplastic elastomers will be presented. As a experimental part of work, preparation of thin films from thermoplastic elastomeric materials will be followed by evaluation of air permability characterisation with regards of used materials and employed process technology modification.

Forma zpracování bakalářské práce: **tištěná/elektronická**
Jazyk zpracování: **Angličtina**

Seznam doporučené literatury:

1) Biron, Michel. (2018). *Thermoplastics and Thermoplastic Composites (3rd Edition)*. Elsevier.
2) McKeen, Laurence W.. (2017). *Permeability Properties of Plastics and Elastomers (4th Edition)*. Elsevier.
3) Durling, Warren. (2017). *Extrusion Coating Manual (5th Edition)*. Technical Association of the Pulp & Paper Industry (TAPPI).

Vedoucí bakalářské práce: **doc. Ing. Tomáš Sedláček, Ph.D.**
Ústav inženýrství polymerů

Datum zadání bakalářské práce: **2. ledna 2023**
Termín odevzdání bakalářské práce: **19. května 2023**

L.S.

prof. Ing. Roman Čermák, Ph.D. v.r.
děkan

Ing. Jana Navrátilová, Ph.D. v.r.
ředitel ústavu

Ve Zlíně dne 10. února 2023

PROHLÁŠENÍ AUTORA
BAKALÁŘSKÉ PRÁCE

Beru na vědomí, že:

- bakalářská práce bude uložena v elektronické podobě v univerzitním informačním systému a dostupná k nahlédnutí;
- na moji bakalářskou práci se plně vztahuje zákon č. 121/2000 Sb. o právu autorském, o právech souvisejících s právem autorským a o změně některých zákonů (autorský zákon) ve znění pozdějších právních předpisů, zejm. § 35 odst. 3;
- podle § 60 odst. 1 autorského zákona má Univerzita Tomáše Bati ve Zlíně právo na uzavření licenční smlouvy o užití školního díla v rozsahu § 12 odst. 4 autorského zákona;
- podle § 60 odst. 2 a 3 autorského zákona mohu užít své dílo – bakalářskou práci nebo poskytnout licenci k jejímu využití jen s předchozím písemným souhlasem Univerzity Tomáše Bati ve Zlíně, která je oprávněna v takovém případě ode mne požadovat přiměřený příspěvek na úhradu nákladů, které byly Univerzitou Tomáše Bati ve Zlíně na vytvoření díla vynaloženy (až do jejich skutečné výše);
- pokud bylo k vypracování bakalářské práce využito softwaru poskytnutého Univerzitou Tomáše Bati ve Zlíně nebo jinými subjekty pouze ke studijním a výzkumným účelům (tj. k nekomerčnímu využití), nelze výsledky bakalářské práce využít ke komerčním účelům;
- pokud je výstupem bakalářské práce jakýkoliv softwarový produkt, považují se za součást práce rovněž i zdrojové kódy, popř. soubory, ze kterých se projekt skládá. Neodevzdání této součásti může být důvodem k neobhájení práce.

Prohlašuji,

- že jsem na bakalářské práci pracoval samostatně a použitou literaturu jsem citoval. V případě publikace výsledků budu uveden jako spoluautor.
- že odevzdaná verze bakalářské práce a verze elektronická nahraná do IS/STAG jsou obsahově totožné.

Ve Zlíně, dne:

Jméno a příjmení studenta:

.....
podpis studenta

ABSTRAKT

Tato bakalářská práce se zabývá různými možnostmi modifikací bariérových vlastností polymerních materiálů s možností využití pro tento účel nanoplniv. Modifikace, které se ukázaly dle literární rešerše jako velmi efektivní a zároveň pro nás proveditelné byly odzkoušeny s termoplastickým polyurethanem (TPU) jako výchozí modifikovaný materiál s dobrými bariérovými vlastnostmi i v čistém stavu. Jako plniva byly zvoleny dva typy montmorillonitu (MMT) a dva druhy grafen oxidu (GO). Z těchto směsí byly vyfouknuty fólie, které byly dále testovány nejen na plynopropustnost, ale i X-Ray Diffraction (XRD), který ukázal stupeň rozdispergování nanoplniva, reologické měření hodnotící změny procesních vlastností tavenin, Diferenční skenovací kalorimetrie (DSC), ze které byly zhodnoceny změny v teplotě tání a krystalizace v závislosti na přidání plniva, a nakonec Dynamická mechanická analýza (DMA), která popsala viskoelastické chování modifikovaných materiálů v pevné fázi.

Klíčová slova: plynopropustnost, bariérové vlastnosti, nanoplniva, termoplastický elastomer

ABSTRACT

This bachelor thesis deals with various possibilities of modification of barrier properties of polymeric materials with the possibility of using nanofillers for this purpose. The modifications that proved to be very effective according to the literature search and also practicable for us were tested with thermoplastic polyurethane (TPU) as the initial modified material with good barrier properties even in the pure state. Two types of montmorillonite (MMT) and two types of graphene oxide (GO) were chosen as fillers. Films were blown from these blends and were further tested not only for gas permeability but also by X-Ray Diffraction (XRD), which showed the level of dispersion of the nanofiller, rheological measurements evaluating changes in the process properties of the melts, Differential Scanning Calorimetry (DSC), from which changes in melting and crystallization temperature as a function of filler addition were evaluated, and finally Dynamic Mechanical Analysis (DMA), which described the viscoelastic behavior of the modified materials in solid phase.

Keywords: gas permeability, barrier properties, fillers, thermoplastic elastomers

I would like to thank my supervisor doc. Ing. Tomáš Sedláček, PhD. for his support, guidance and patience. Also, I would like to thank my family for their support during my studies and during the time I have been writing this thesis.

I hereby declare that the print version of my Bachelor's/Master's thesis and the electronic version of my thesis deposited in the IS/STAG system are identical.

CONTENTS

INTRODUCTION **9**
I THEORY **10**
1 GAS PERMEABLITY **11**
2 ELASTOMERS AND THEIR APPLICATIONS **12**
2.1.1 Thermoplastic polyurethane (TPU) 12
3 MODIFICATION OF POLYMER BARRIER PROPERTIES **14**
3.1 MULTILAYER PRODUCTS 14
3.2 SURFACE MODIFICATION 14
3.3 NANOFILLERS 15
3.3.1 Nanoclay 15
3.3.2 Carbon nanoparticles 17
3.3.3 Other nanoparticles 19
3.4 MODIFICATION OF GAS PERMEABILITY UNDER PERMANENT DEFORMATION 19
4 TESTING METHODS **21**
4.1 WIDE ANGLE X-RAY SCATTERING (WAXD) 21
4.2 RHEOLOGICAL TESTING 21
4.3 DIFFERENTIAL SCANNING CALORIMETRY (DSC) 22
4.4 DYNAMIC MECHANICAL ANALYSIS (DMA) 22
4.5 GAS TRANSMISSION RATE TESTING 23
II ANALYSIS **24**
5 SAMPLES PREPARATION **25**
5.1 MATERIALS 25
5.2 COMPOUNDING 25
5.3 BLOWING 28
6 XRD - WAXD **30**
6.1 RESULTS AND DISCUSSION 31
7 RHEOMETER **38**
7.1 RESULTS AND DISCUSSION 39
8 DSC **46**
8.1 RESULTS AND DISCUSSION 47
9 DMA **52**
9.1 RESULTS AND DISCUSSION 53
10 GTR TESTING **54**
10.1 RESULTS AND DISCUSSION 54

CONCLUSION **57**
BIBLIOGRAPHY **58**
LIST OF ABBREVIATIONS **63**
LIST OF FIGURES **64**
LIST OF TABLES **66**

INTRODUCTION

Gas permeability is a property of a material characterized by the amount of gas that passes through the sample area in a specified time. Gas permeability is not a constant for a particular material, it varies with the gas used and the ambient conditions. We are interested in this property in many applications, such as the food industry, specifically packaging materials, and the automotive industry, where materials with barrier properties are used to make tyres or tubes. Another application is the pharmaceutical industry where barrier properties are used together with the stiffness and chemical inertness of the material, such applications are, for example, tubes that connects the infusion to the cannula or packaging.

Materials with maximum barrier properties are glass and metals. In the packaging industry, packaging with an aluminium coating is used to keep the packaged product in an inert atmosphere. The disadvantage of these materials is that they are non-deformable and more complicated to recycle, so nowadays there is an increasing switch to thermoplastic materials. Some of these materials have good barrier properties on their own and are also deformable and can be easily modified due to their easy processability. Examples of such materials are thermoplastic polyurethane (TPU) or poly(dimethylsiloxane) (PDMS).

As already mentioned, their properties can be modified quite efficiently. This can be done by adding fillers such as micro and nanofillers, for example nanoclay, graphene, or, from renewable and easily recyclable materials, cellulose. Another possible modification is to layer a material with barrier properties on a substrate with lower barrier properties. Again, these films can be metals, which are applicable to products not subject to deformation, or thermoplastic elastomers such as, for example, TPU, which can be used to deformated materials because of its flexibility. Due to the variety of modification options, some of which for modification barrier properties will be mentioned below, thermoplastic materials are increasingly being applied.

I. THEORY

1 GAS PERMEABLITY

Gas permeability is one of the physical properties of a material. It is determined under given conditions of temperature and pressure and measures the flow through a polymer membrane of a defined size. It is influenced by the chemical structure of the polymer and by the type of gas (air, nitrogen, CO_2, etc.). Therefore, the gas permeability is not a material constant, but always depends primarily on the gas used and then on the ambient conditions such as pressure, temperature and whether the material is in a deformed state. [1]

Materials such as metals and glass have excellent barrier properties. However, they are not as widely used as plastics, which surpass them in their simplicity of processing. Of the plastics used for packaging materials and in the automotive industry, where reversible deformation is needed, these are mainly thermoplastic elastomers (TPEs), that are characterized by their reversible deformation and, although they do not have high barrier properties on their own, they can be easily modified to improve these properties. TPEs are also more flexible, better processable and more readily available than metal or glass.

Applications for which barrier properties are crucial are for example packaging films, wheel tubes or protective films. Nowadays, many methods are known to improve the barrier properties and research continues. In general, various fillers can be used to reduce the gas permeability, most often nanoclay or carbon nanoparticals. High level of dispersion of these nanofillers is very important to ensure efficient modification. [2]

2 ELASTOMERS AND THEIR APPLICATIONS

Elastomers are generally materials that exhibit both viscous and elastic behavior and are so-called viscoelastic. They are also characterized by large reversible deformation and a cross-linked structure. They are divided into two groups, thermoplastic and thermoset elastomers. [3]

Thermoset elastomers are cross-linked polymers, this crosslinking occurs by vulcanization in the presence of a vulcanizing agent such as sulfur or peroxide. This strong network makes it impossible to melt or reshape. [3]

Thermoplastic elastomers have physical network, which is weaker than that of thermosets. Due to this weaker network, they exhibit the strength, durability and reversible deformation of thermosets, but unlike thermosets they can be processed repeatedly. Some are also characterised by good barrier properties and are also easier to recycle, which is the direction today's developments are taking. [3]

Thanks to flexibility, transparency, chemical inertness, low specific weight, and low cost in respect to traditional materials such as glass, metal, they replace metals and other materials in many applications. [4] After modification of their barrier properties and due to their transparency and flexibility, they are preferably used in the packaging industry. In the automotive industry, they are gaining prominence due to their better processability and better recyclability. Materials such as thermoplastic polyurethane, for example, have good barrier properties even without the addition of fillers, and with a small amount of nanofillers (up to 5 wt.%) their barrier properties can be increased by up to 80%. [5]

Other uses of thermoplastic elastomers can be in medicine for tubes that connects the infusion to the cannula, infusion packaging, etc., as filaments for 3D printers, or for making animal tags for identification. [6]

2.1.1 Thermoplastic polyurethane (TPU)

Thermoplastic polyurethane is generally obtained by reacting polyol with polyisocyanate and other components such as chain extenders, which are used to control its thermoplastic properties. [7]

Thanks to their properties such as toughness, abrasion resistance, low coefficient of friction and good barrier properties, they have found applications in many industries. The hardness of TPU reaches a high end (80 Shore A) but can be modified to have lower values. And by

adjusting the ratio of rigid to soft phase, different types of TPUs can be created, such as non-flammable types, self-healing, or PU with shape memory. [8]

As block copolymers they are resistant to non-polar solvents such as fuels, oils, and greases. Conversely, it is poorly resistant to polar solvents. They are widely used in many technical applications such as coatings, paints, foams, and elastic fibers. [8]

3 MODIFICATION OF POLYMER BARRIER PROPERTIES

Polymers can be modified in various ways to improve their properties. Modifications can improve their mechanical resistance, electrical properties, thermal stability, chemical resistance, etc. Modifications can be provided by the addition of nanofillers such as nanoclay, carbon black, graphene oxide, etc.; microfillers, and another option is to coat the surface of the material or coextrusion with another material that provides, for example, barrier properties, better conductivity, or thermal resistance.

Barrier properties can be improved in various ways. There is a lot of research going on in this area to make the material as gas and moisture impermeable as possible. One very presented possibility is production of multilayer products, application of active surface coating and modification by using nanofillers, which can be of different shapes and sizes - the most commonly used nanofillers include graphene oxide (GO) and nanoclay.

3.1 Multilayer products

Coextrusion can be used as another method to apply the film to the substrate. Many layers of film can be applied by this method and at 65 layers the barrier properties were improved by 75 %. These layers were made of TPU, which is flexible, so it retained its barrier properties even at 300% deformation. [9]

3.2 Surface modification

Another option for modifying the barrier properties is to apply a film onto a substrate. The effect of this modification is not as great as the modification by adding filler. Big advantage of these modification is connected with the fact that some of such solutions proven to be a good barrier even in deformation as it is discussed below. Its deposition is complex, the subsequent adhesion to the substrate is crucial for the modification of the properties.[34] Graphene [35], wolfram carbide or chromium [36] can be used as films. Deposition of graphene films is complex and has only been done on the millimeter scale so far. Wolfram carbide and chromium were applied to the fluoroelastomer by ion implantation in a vacuum chamber. The modified material improved its barrier properties to nitrogen by 30%.

3.3 Nanofillers

Nanofillers added to the polymer improve its mechanical properties, thermal and dimensional stability, gas permeability, fire and chemical resistance or, for example, optical and electrical properties. The amount of nanofiller added is usually up to 5 wt.%, which is sufficient for modification. The nanofiller forms a transition region with the matrix, the interphase, which represents the majority of volume of the composite and so has a major influence on the final properties. The size of this interphase, and hence the interaction between the nanoparticles and the filler and the final properties, depends on entanglement of the polymer chains, the surface energy of the nanoparticle and the flexibility of the polymer chain. For better distribution of nanoparticles, its surface is modified, and thereby more chains can attach on the particle and the modification of final properties is more effective.[2]

Nanoparticles can be of different shapes, for example, plates, lamellae or spheres, their distinguishing characteristic is at least one dimension at the nanoscale. They are derived from natural clay minerals and have the structure of sheet-like hydrous silicates known as phyllosilicates. [2]

3.3.1 Nanoclay

Nanoclays are derived from natural clay minerals and have the structure of sheet-like hydrous silicates known as phyllosilicates. They can be divided into four groups, namely kaolinite, monmorillonite/smectite, illite and chlorite groups, which differ in crystal structure. Of those listed, the most studied are montmorillonites, which are characterized by their 2:1 sheet-structure, an octahedral sheet of alumina lies between two tetrahedral sheets of silica sharing their apex oxygen atoms, SiO_4 groups of tetrahedral sheets are linked to form a hexagonal network. These three structures form a single layer of clay called tactoid, which has a characteristic thickness of 1 nm. The tactoids are separated from each other by a van der Waals gap, which is generally called the interlayer. The presence of cations in this interlayer makes montmorillonite hydrophilic and incompatible with most hydrophobic polymers; to avoid this possibility, the silicate layers are organically modified. When clay is incorporated into the polymer matrix, two states can occur, the first is intercalation, where expansion of the silicate layers is observed, the second is exfoliation, which involves penetration of the polymer and delamination of the silicate tactoids. For best property improvement, exfoliation must occur. [2] However achieving exfoliation is not easy and depends a lot on the preparation method of nanocomposite. The basic methods are in situ

template synthesis, intercalation of polymer from solution, in situ polymerization, and melt intercalation. [2, 10]

The first method consists of synthesizing clay inside a polymer matrix using general sol-gel techniques, which means that clay crystals nucleate and grow in the matrix and polymer chains are enclosed within the layers. [2]

The second method uses the exfoliation of clay into layers in a solvent in which the polymer used is soluble. This technique is used to form intercalated nanocomposites such as polyvinyl alcohol, poly(ethylene oxide) (PEO), or polyacrylic acid. It consists of intercalating the dissolved polymer between clay layers and then removing the solvent, resulting in the closing off of the filler chains between the clay layers. [11–13] This method of incorporating the filler into the polymer is described in [12, 13], where brominated butyl rubber (BIIR) and chlorobutyl rubber (CIIR) were used as the starting modified materials. In [12], organoclay was used as a filler and both intercalation and exfoliation occurred, barrier properties measured for O_2 at a filler concentration of 5 phr (parts per hundred of the rubber) achieved a 53% improvement. Sample preparation was carried out by dissolving the rubber in hexane at 50 °C for 3 h followed by mixing with the filler solution, washing with water and drying. In this study [13], the relationship between the solubility parameter and the resulting properties was investigated. Cyclohexane was reported as the best solvent. According to XRD, the greatest filler intercalation occurred when using this solvent. The nanocomposite of CIIR and Coloisite 15 A (5 phr) improved its barrier properties to N_2 compared to pure rubber by 70%, depending on the decreasing differences between the interactions of CIIR and filler with the solvent.

In situ polymerization consists of swelling the modified silicate layers with a liquid monomer solution and subsequent polymerization in the interlayer. [2] This method of incorporation was investigated, for example, in reference [14], where it was confirmed that intercalation, even exfoliation, occurred by this method of preparation. Thermoplastic polyurethane (TPU) was chosen as the initial modified material and clay was added at a concentration of 5.3 wt.%. This modified material increased the barrier properties for CO_2 by 40%.

The most commonly used method is direct incorporation of nanoparticles into the polymer matrix, where their compatibility and mixing conditions play a major role. Depending on the process, intercalation or even exfoliation occurs. [15–18]. References [15, 19, 20] test this method of mixing the filler using a twin-screw extruder into the polymer and then measuring the change in gas permeability for O_2. In [15] ,biodegradable polyurethane was used as a

modified polymer, nanofiller was added at concentrations of 3, 5 and 7 wt.% and mixed into the polymer matrix. X-ray diffraction (XRD) measurements confirmed that the filler was both intercalated and partially exfoliated in the matrix. Gas permeability was measured on blown films and the best barrier properties were measured for mixtures with a filler concentration of 3 wt.%. The melt mixing method of filler and polymer was also used in [19], where the organoclay was partially exfoliated and uniformly dispersed into polyether block amide (PEBA). Nanocomposites were prepared at concentrations of 1, 3, 5, 7 and 10 wt.%, with the best barrier properties measured for the 7% concentration for which the oxygen transmission rate (OTR) [cc/m2.day] dropped from 4000 to 1000. Cloisite 30 B nano-clay was used as filler in reference [20], where very little intercalation occurred, and therefor barrier properties were improved by less than 8 %.

In [18], N_2 was used as the test gas and montmorillonite (MMT) as the filler. In this case, only a 25 % improvement was obtained.

The effect of the length/width ratio of nanoparticles on gas permeability, specifically for CO_2, was also investigated in reference [10]. Measurements were made for a particle size ratio of 2000 and plotted as a dependence of the gas permeability parameter P on the volume fraction of filler. Subsequently, the curve equation was used to calculate the curve for a ratio of 20 and for a ratio of 192, for which the measurements came out surprisingly well, as much higher values were expected, since the exfoliated structure appeared just for the ratio of 2000, and had very good barrier properties. [10]

3.3.2 Carbon nanoparticles

By adding these particles, properties such as mechanical and thermal properties can be improved. This group includes carbon nanotubes, graphene nanoplatelets, carbon nanofibers (CNFs) and carbon black, all of which have been extensively researched. [2]

3.3.2.1 Graphene

Graphene is a single layer of graphite in which these layers are held together by van der Waals forces. It is characterized by its 2D honeycomb structure of sp2 hybridized carbon atoms. Due to this structure, it achieves high in-plane electrical conductivity, high Young's modulus and stenght and high thermal conductivity. Graphene is very difficult to exfoliate from graphite, there are several methods: peeling method, that allows obtaining high-quality crystallites, insertion chemical species between graphene sheets, using intercalation agents

followed by microwave heating, last method is graphite oxidation to obtain exfoliated graphene oxide (GO). [2]

To improve intercalation in the matrix, graphene and GO are chemically functionalized using various chemical species such as amines, isocyanates, diisocyanates, or alkyl lithium reagents. [2]

Graphene can be incorporated into the matrix in different ways, the first is in situ intercalative polymerization, the next is solution intercalation [5, 21–27], and finally melt intercalation [28–30].

The materials in the following references [5, 21, 22, 31, 32] were prepared by solution mixing method. Poly(dimethylsiloxane) (PDMS) [21] was used as the polymer for modification and 0.43 vol.% GO was added. The barrier properties of the formed nanocomposite were measured for CO_2 and N_2 and improved by 45%. For the modification of SEBS [22], 7.5 wt.% FG was used and exfoliated, the barrier properties measurement showed an improvement of 79 %. In [5], natural rubber (NR), styrene butadiene rubber (SBR) and PDMS were used as modification materials and 5 wt.% functionalized graphene was added to each. All these compounds showed very similar behaviour and the air barrier properties were improved by 80 %. The modification of the fluoroelastomer with GO is described in [31]. The suspensions prepared were mixed dropwise, and the filler was 5 wt.% in the resulting mixture. The oxygen permeability was reduced by 79 % compared to the pure material. To improve the barrier properties to O_2, grafted maleic anhydride IIR [32] was modified. Concentration of graphene added to IIR was 5 phr and gas permeability was reduced more than when nanoclay was added (which was also measured), but even so the improvement was not significant.

The last option, which is intercalation of graphene by melt mixing, was used to prepare the samples in reference [33] were prepared by melt mixing and subsequent pressing. EPDM here was modified with 7 phr graphene. Exfoliation occurred and the oxygen barrier was improved by 47 %.

3.3.2.2 Carbon nanofibers and nanotubes

Carbon nanofibers are also surface functionalized before incorporation into the matrix, this can be done by oxidation with a strong acid, that makes the fibers dispersible in water. [2]

The CNFs can be produced in a reactor at 1100 °C in the presence of natural gas (CH_4), $Fe(CO)_5$ and H_2S. The iron particles produced by the decomposition of $Fe(CO)_5$, after activation by sulphur, act as catalysts for the growth of the nanofibers. Other production methods are electrospinning of the polymer or chemical vapor deposition. [2]

3.3.2.3 Carbon black

The structure of carbon black is a mixture of amorphous carbon and crystalline or semi-crystalline graphite-like structures in which the graphene layers are distorted. Its resulting electrical properties depend on the presence of the crystalline phase. For this nanofiller to provide the best mechanical properties, its particles must be very small with a large surface area and must be well dispersed in the matrix. The incorporation of these nanoparticles can be done in the same ways as for nanoclays. [2]

3.3.3 Other nanoparticles

Other nanoparticles used to modify the properties of polymers include nano-oxides: silica (SIO_2), alumina (AL_2O_3) and titania (TiO_2), nanocarbides, which are hard materials typically used as refractories due to their high melting points or as abrasives in powder form. Finally, organic nanofillers: cellulose, nanolignin, chitin. These are being explored mainly due to the growing interest in the environment, ecology and renewable resources. [2]

3.4 Modification of gas permeability under permanent deformation

For many applications there is a need to maintain barrier properties even when the material deforms, an example of such an application would be wheel tubes. The most common material treatments for this end use are films deposited on the base material. It is generally very difficult to achieve adequate barrier properties and maintain them while repeatedly deforming the product.

TPU is used as the surface film or substrate because of its good barrier properties. [9, 36, 37] There are several ways of applying films to a substrate, the first way may be to cast a polymer wafer and then transfer it to the substrate with final edge dressing for a better seal as shown in [37]. This method is very challenging and despite improving barrier properties and retaining them even in the deformed state, it is not recommended for routine applications. After several cycles of stretching and relaxing, the gas permeability increased significantly.

Another method may be to apply layers of film by gradual dip coating. Products made this way with four layers applied retain their barrier properties up to 15% deformation, higher deformations are critical as they found out in [36].

4 TESTING METHODS

The following methods were used to analyze and characterize the various properties of the samples. The most important characterization was gas permeability, which was modified. Other methods were DSC, DMA, Rheometer and X-ray analysis.

4.1 Wide angle X-ray scattering (WAXD)

This method can be used to determine crystallinity, density of the crystalline phase, level of intercalation/exfoliation of fillers, or to estimate the size of crystallites. Solid and powder forms of materials as well as thin films can be tested. [38]

When radiation interacts with the material, it is either reflected or absorbed. In reflection, if the reflected wave has the same wavelength, it is called elastic reflection. The captured reflected beam is then evaluated by the system and the entire measurement is processed into a graph as a dependence of intensity on the angle 2Θ. [38]

This analysis allows us to determine whether the filler has intercalated or even exfoliated in the matrix. Intercalation results in a shift of peaks to lower angle values, while exfoliation results in the complete disappearance of the peaks. [38, 39]

X-ray measurement is described by many standards, depending on the material being measured and whether it is Wide-Angle X-Ray Diffraction (WAXD) or Small-Angle X-Ray Diffraction (SAXD). The standard describing X-ray diffraction of polycrystalline and amorphous materials is DS/EN 13925-1: Non-destructive testing - X-ray diffraction from polycrystalline and amorphous material - Part 1: General principles. [40]

4.2 Rheological testing

Rheometry measures the amount of deformation a material or liquid undergoes when a force is applied and measures its viscoelastic properties, such as viscosity, storage modulus, loss modulus, etc, and determine the properties of melt that are important for the subsequent processing of the material. [41] Different methods can be used in these tests. They differ in whether only the top part rotates (stress-controlled) or whether both the top and bottom part rotate (strain-controlled). Another measurement parameter is the rotation method of the bob. It may rotate all the way around, which is called rotational testing, or it may only move in small angles to the right and left, this is oscillatory testing. Rotational testing is used more for liquid samples and oscillatory testing for solid samples. [42]

Rheological measurements are generally specified by different standards depending on the type of rheometer (oscillating, rotary, capillary) and the type of material to be measured. An example of a standard that deals with the measurement of dynamic mechanical properties of plastics, most commonly in the frequency range of 0.01 to 100 rad/s, on an oscillatory rheometer is ISO 6721-10: Plastics - Determination of dynamic mechanical properties - Part 10: Complex shear viscosity using a parallel-plate oscillatory rheometer. [43]

4.3 Differential Scanning Calorimetry (DSC)

It is a thermoanalytical technique in which the difference in the amount of heat required to increase the temperature of a sample and reference is measured as a function of temperature [44]. This method is used to measure melting temperature, crystallization temperature, glass transition temperature, denaturation temperature, crystalline phase content and specific heat or heat capacity. Temperatures defining the phase changes of a material are important for the correct adjustment of temperature conditions during processing and application.

Measurements are made in the presence of an inert atmosphere and two pans, one empty, reference, the other containing the sample under test. Each pan has its own heating device which must change temperature at the same rate.[45]

DSC measurements are regulated by different standards depending on the parameters and materials being measured. For example, one of the standards is ASTM E537-12: Standard Test Method for The Thermal Stability of Chemicals by Differential Scanning Calorimetry, which specifies conditions for measuring the thermal stability of chemicals based on enthalpy changes. [46] ASTM E1356-08(2014): Standard Test Method for Assignment of the Glass Transition Temperatures by Differential Scanning Calorimetry describes the measurement of the glass transition temperature by DSC and the subsequent evaluation of, for example, thermal history and mechanical and electrical properties.[47]

4.4 Dynamic Mechanical Analysis (DMA)

DMA refers to response of plastic materials when they are subjected to dynamic or cyclic forces. Specimens can be tested in tension and bending, at various high and low temperatures depending on the properties of the tested material. This is material property knowledge describing the temperature and frequency dependence of the mechanical response of a product to mechanical stress in the case of its actual application.

Measurements are regulated by different standards depending on what we want to measure and by which method. For example, ASTM E2425-21: Standard Test Method for Loss Modulus Conformance of Dynamic Mechanical Analyzers provides rules for measuring loss modulus on a variety of commonly available DMA instruments [48]. ISO 6721-11: Plastics - Determination of dynamic mechanical properties - Part 11: Glass transition temperature specifies methods for determining the glass transition temperature and the types of materials for which measurements can be provided [49].

4.5 Gas Transmission Rate testing

In general, measuring of GTR can be used to define barrier properties of foils. This measurement can be performed by different methods depending on the measurement standard chosen. The first method consists of measuring the pressure change after one of the chambers has been evacuated of air to the maximum extent possible and the gas to be measured is at atmospheric pressure in the other. The second method is that the pressure in the air-filled chamber is higher than atmospheric pressure and the pressure in the first chamber is atmospheric pressure. Again, the change in pressure is recorded.

Both of these measurements are described in the following standards: ČSN EN ISO 2556: Plastics - Determination of the gas transmission rate of films and thin sheets under atmospheric pressure - Manometric method, which describes measurements where one chamber contains the gas to be measured at atmospheric pressure and the other is evacuated from the gas at zero pressure, ASTM D1434-82: Standard Test Method for Determining Gas Permeability Characteristics of Plastic Film and Sheeting, which describes both the manometric and volumetric methods, where in both methods one chamber is filled with a high pressure gas and the other chamber is either completely free of gas (manometric method) or filled with atmospheric pressure gas (volumetric method).

II. ANALYSIS

5 SAMPLES PREPARATION

First, concentrated mixtures of TPU matrix and our selected fillers were prepared, these were two types of GO (graphene oxide) and two types of MMT (montmorillonite). Two kilograms of each mixture were prepared from each species, each at a concentration of 20wt.% for the mixture with MMT, the mixtures with GO were prepared from each species at two concentrations, namely 20wt.% and 10wt.%. The lower concentration was chosen to continue with, the higher concentration was not, because of its great difficulty in processing.

Afterwards, the concentrated mixtures were added to the pure TPU for blowing in specific ratios to give the new mixtures concentrations of 5 and 10 wt.% for MMT and concentrations of 3 and 5 wt.% for the two GO species.

5.1 Materials

Two types of GO and two types of MMT were used for sample preparation. The types of GO were as follows ES 100 C10 (GO 1) and ES 500 F5 pH (GO 2). The MMTs available were 15A and 30B. The TPU for masterbatch preparation was Pearlthane 11T80 and for blowing was Pearlthane ECO D12T80E. The materials were dried at 80 °C for 3 hours before each treatment. GO types have very similar properties and differ only in temperature resistance, GO 2 degrades at lower temperatures.

The MMT 15 A and 30 B fillers are not significantly different, have the same particle size, 90 % <= 13 um, 50 % <= 6 um and 10 % <= 2 um, the same hardness, Shore D, and contain the same maximum moisture content, 2 %. They differ in Specific Gravity, which is 1,66 g/cc for 15 A and 1,98 g/cc, and in Bulk Density, which is 0,1729 g/cc for 15 A and 0,2283 g/cc for 30 B. [50, 51]

5.2 Compounding

Mastebatch mixtures were processed on a twin-screw compounder at different conditions according to the fillers. The compounder and granulating machine were supplied by LAB TECH ENGINEERING COMPANY LTD (Fig. 1, 2).

Figure 1: Compounding machine.

A granulating machine was first attached to the compounder, which was subsequently shut down because the strings were sticking to the granulating unit and the material could not be fully processed. Granulation was carried out straight from the melt with water cooling and air drying. (Fig. 2, 3)

Figure 2: Granulation machine

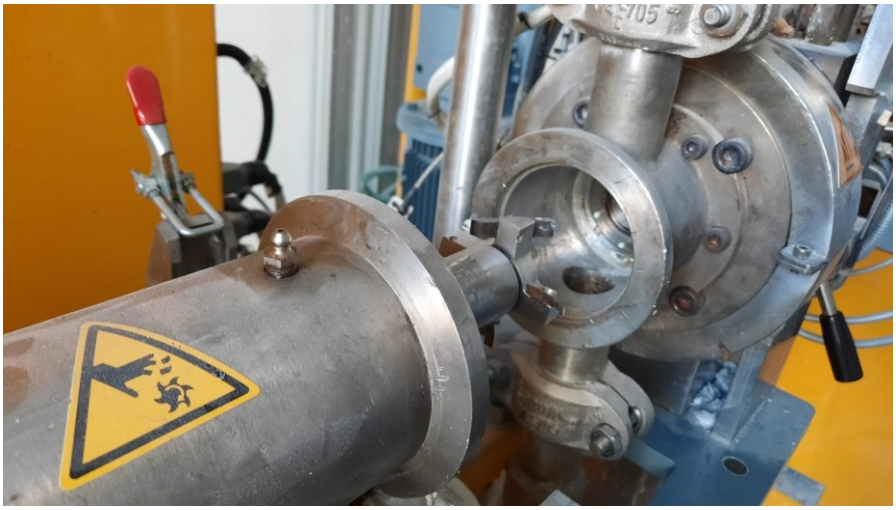

Figure 3: Detail of granulating head

The first mixtures with MMT types were processed well, with the following conditions (from hopper to extrusion head): 136, 155, 168, 169, 171, 172, 174, 174, 176, 180, 174 and 175 °C. (Fig. 4).

Figure 4: Extrusion conditions of TPU 11T80 with MMT fillers

When processing mixtures with GOs at a concentration of 20 wt.% difficulties were encountered, the material did not granulate well and suitable conditions were not found. Therefore, it was tried to process mixtures with a lower concentration, in particular 10 wt.%. Only GO 2 could be processed in this way, type GO 1 could not be processed. GO 2 was processed under the following conditions (from hopper to extrusion head): 136, 147,153, 154, 155, 153, 146, 145, 146, 145, 118 and 129 °C. (Fig. 5)

Figure 5: Extrusion conditions of TPU 11T80 with GO 2 filler

5.3 Blowing

Masterbatches were dried before blowing, as well as plain TPU ECO D12T80E (TPU ECO). Blowing was carried out on a BOCOMATIC EB 25 machine (Fig. 6). Different concentrations of mixtures were prepared for blowing. A new mix of 300 g was prepared for all concentrations and all masterbatches. For the MMT masterbatch, concentrations of 5 and 10 wt.% were prepared, corresponding to TPU ECO and 20% masterbatch ratios of 3:1 and 1:1, respectively. Starting from MMT 15A only 5% mixture was processed, while from MMT 30B both concentrations were processed. Masterbatch with GO 2 (10 wt.%) was mixed at 3 and 5 wt.% concentrations, corresponding to TPU and GO ratios of 2:1 and 1:1.

First, pure TPU samples were blown at the following conditions: 155, 170, 165, 158 and 163 °C (Fig. 7). After blowing the required number of samples, the mixtures with MMT were blown at the following conditions: 145, 166, 155, 150 and 155 °C (Fig. 8). When blowing GO 2, the filler was not completely incorporated into the matrix, thus it was not evenly dispersed (Fig. 9) and the blown sleeves cracked. GO 2 could not be blown, hence gas permeability was not measured further for it.

Figure 6: BOCOMATIC EB 25 machine

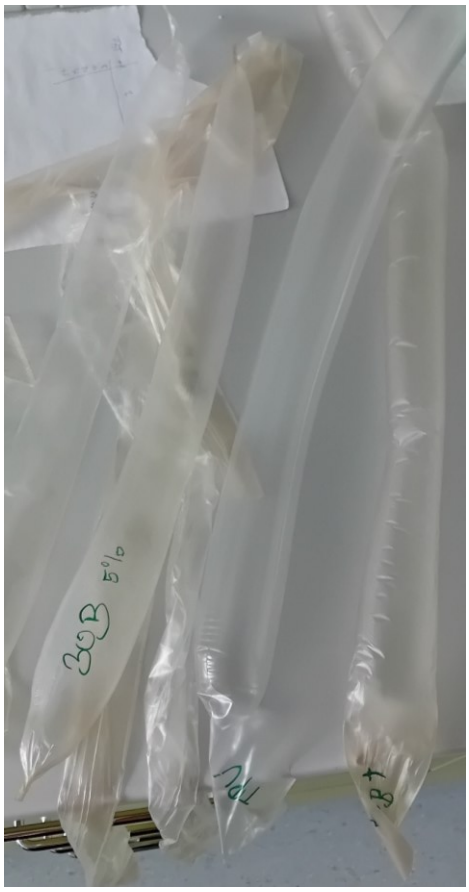

Figure 7: Photo of poor GO 2 filler dispersion in TPU matrix (left picture)

Figure 8: Photo of good MMT filler dispersion in TPU matrix (right picture)

6 XRD - WAXD

This measurement was performed for masterbatches (TPU 11T80 + MMT 15 A/MMT 30 B/GO2), pure TPU 11T80 and TPU ECO D12T80E, and the fillers themselves in powder form. Scanning was performed from a 2Θ angle of 0.7° to 30°, with a step size of 0.025°. Divergence Slit was set to 0.025°. Through the measurements it was possible to determine the level of filler intercalation in the matrix. If itercalation occurs, the peaks shift towards lower angles. [38] Type of machine was XRDynamic 500 (Fig. 9) from Anton Paar. This analysis also determined the proportion of the crystalline phase of the samples.

Figure 9: Anton Paar, XRDynamic 500

6.1 Results and Discussion

6.1.1 TPU 11T80

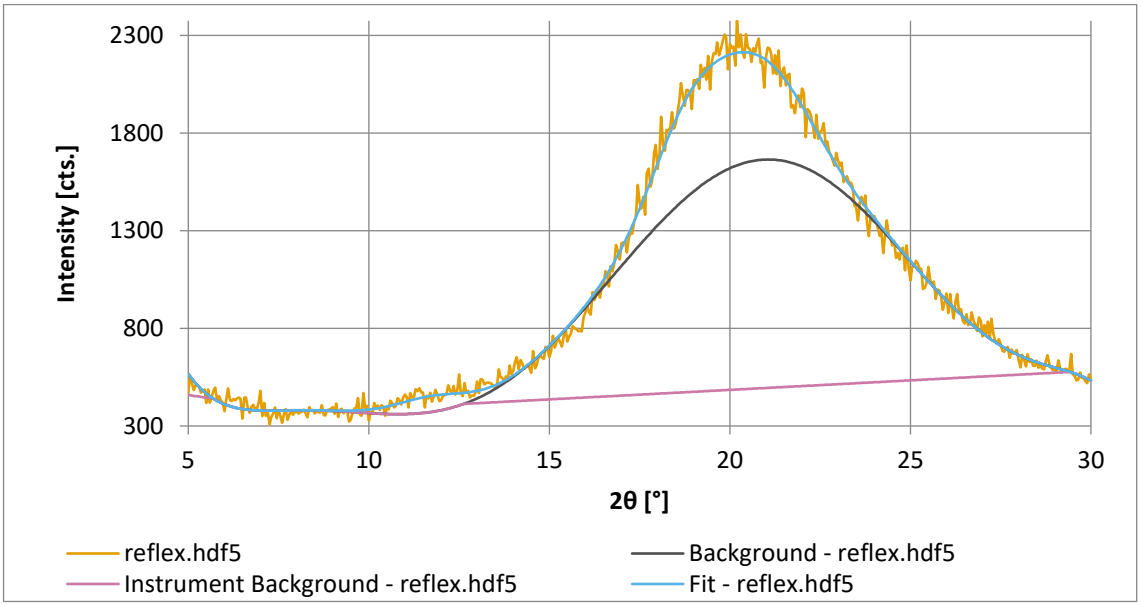

Figure 10: XRD measurement record for pure TPU 11T80, the vertical axis plots the intensity [cts.] and the x-axis plots the angle values 2Θ [°]. The yellow curve shows the course of the measurement itself, the other curves are the result of peaks fitting and backgrounds, and the pink curve shows proportion of amorphous phase.

Table 1: Percentage of crystalline and amorphous phase of TPU 11T80

Phase Type	Area [cts. °]	Rel. Mass [%]
Crystalline	25,84	12,8%
Amorphous	175,93	87,2%

6.1.2 TPU ECO D12T80E

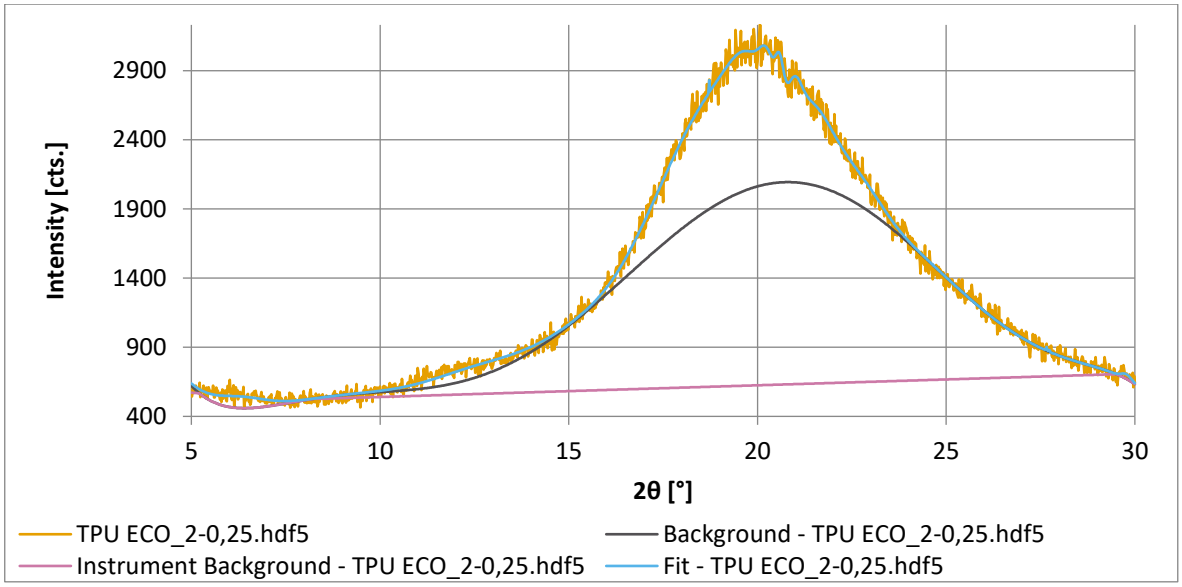

Figure 11: XRD measurement record for pure TPU ECO D12T80E 11T80, the vertical axis plots the intensity [cts.] and the x-axis plots the angle values 2Θ [°]. The yellow curve shows the course of the measurement itself, the other curves are the result of peaks fitting and background, and the pink curve shows proportion of amorphous phase.

Table 2:Percentage of crystalline and amorphous phase of TPU ECO D12T80E

Phase Type	Area [cts. °]	Rel. Mass [%]
Crystalline	81,07	25,7%
Amorphous	234,43	74,3%

Both types of TPU show a clear peak around 20°, more precisely 21.08° for TPU 11T80 and 20.02° for TPU ECO D12T80E (TPU ECO) (Figs. 10, 11). Based on this finding, using these types and mixing them when blowing the films should not be a problem. TPU 11T80 was used to produce masterbatches which were then added to TPU ECO during the blowing process. TPU 11T80 is less crystalline, containing only 12.8 %, TPU ECO contains 25.7 % crystalline phase.

6.1.3 MMT 15 A (powder)

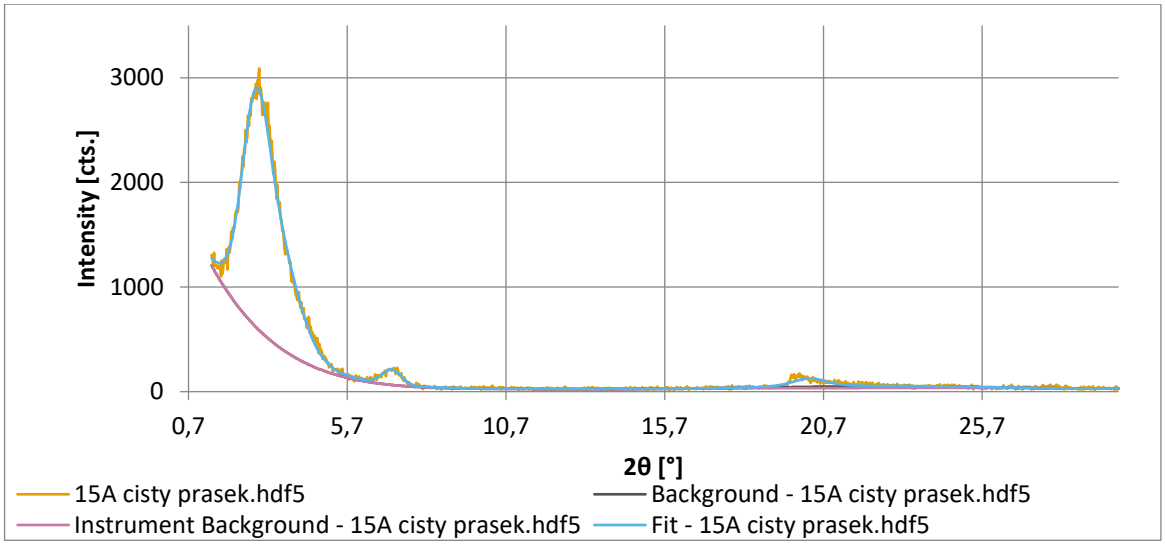

Figure 12: XRD measurement record for MMT 15 A powder, the vertical axis plots the intensity [cts.] and the x-axis plots the angle values 2Θ [°]. The yellow curve shows the course of the measurement itself, the other curves are the result of peaks fitting and background, and the pink curve shows proportion of amorphous phase.

Table 3: Percentage of crystalline and amorphous phase of MMT 15 A powder

Phase Type	Area [cts. °]	Rel. Mass [%]
Crystalline	70,16	97,6%
Amorphous	1,74	2,4%

6.1.4 MMT 15 A + TPU 11T80

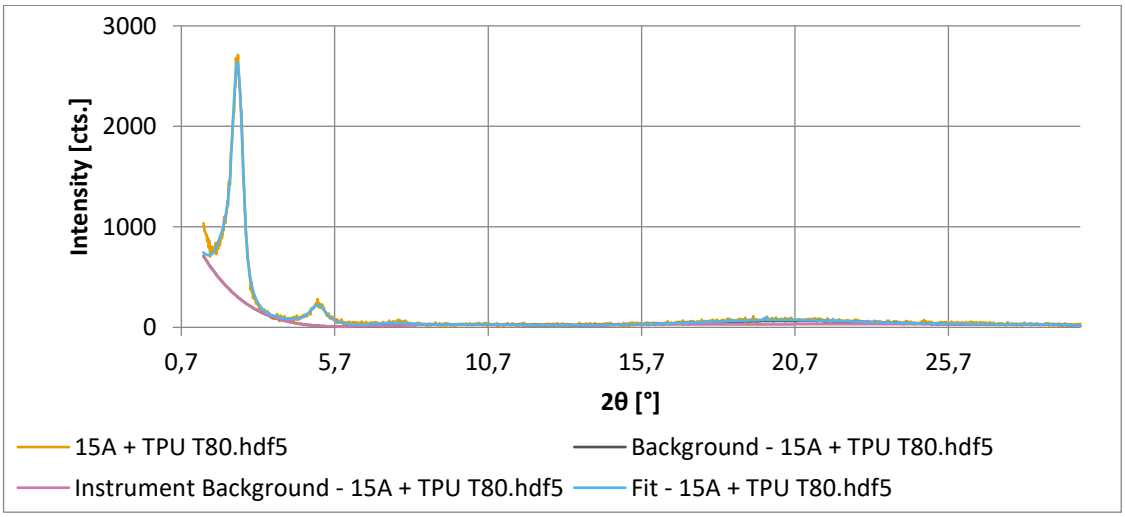

Figure 13: XRD measurement record for MMT 15 A + TPU masterbatch, the vertical axis plots the intensity [cts.] and the x-axis plots the angle values 2Θ [°]. The yellow curve shows the course of the measurement itself, the other curves are the result of peaks fitting and background, and the pink curve shows proportion of amorphous phase.

Table 4: Percentage of crystalline and amorphous phase of MMT 15 A + TPU masterbatch

Phase Type	Area [cts. °]	Rel. Mass [%]
Crystalline	27,62	88,8%
Amorphous	3,48	11,2%

The MMT 15 A filler alone showed (Fig. 12) a significant response at 2.79° and smaller responses at 7.09° and 20.25°. The crystalline fraction of this filler is 97.6 %. This filler blended into the TPU showed (Fig. 13) responses at 2.54°, which contradicts the filler itself, 5.15°, which is the peak that was also shown when testing the filler itself, only it is shifted to the left, and the last response with a peak at 19.92°, but the peak is very broad and low, however it matches the TPU matrix. All the peaks are shifted to the left compared to the pure material results, indicating a slight intercalation of the filler into the matrix. However, if the filler were fully incorporated into the matrix, the shift would be much more significant.

6.1.5 MMT 30 B (powder)

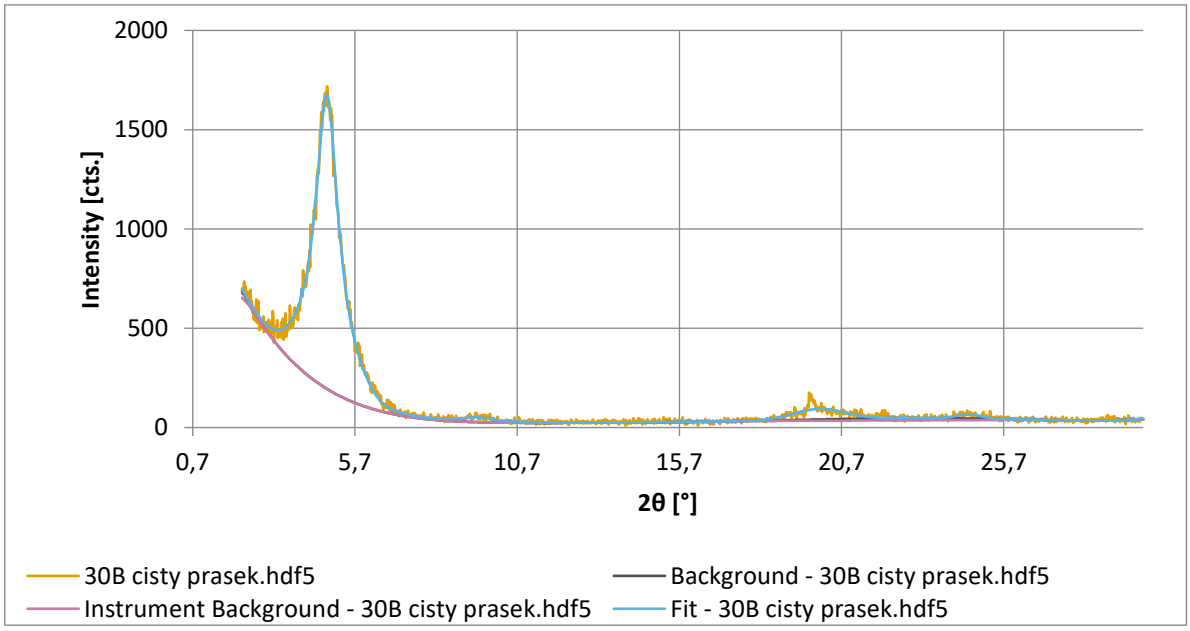

Figure 14: XRD measurement record for MMT 30 B powder, the vertical axis plots the intensity [cts.] and the x-axis plots the angle values 2Θ [°]. The yellow curve shows the course of the measurement itself, the other curves are the result of peaks fitting and background, and the pink curve shows proportion of amorphous phase.

Table 5: Percentage of crystalline and amorphous phase of MMT 30 B powder

Phase Type	Area [cts. °]	Rel. Mass [%]
Crystalline	32,42	96,5%
Amorphous	1,16	3,5%

6.1.6 MMT 30 B + TPU 11T80

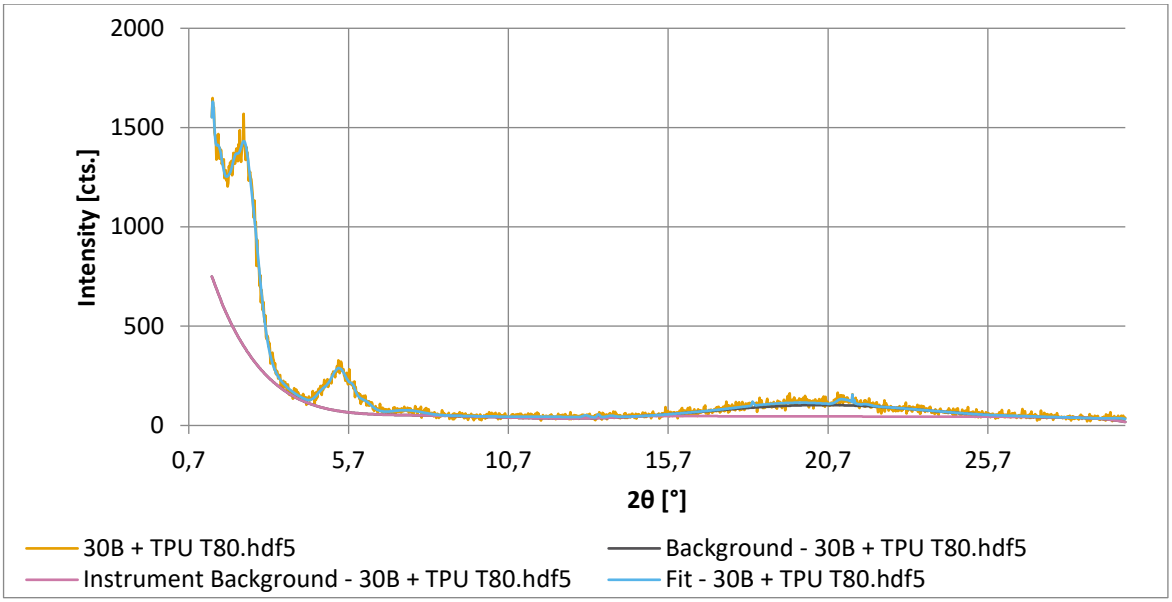

Figure 15: XRD measurement record for MMT 30 B + TPU masterbatch, the vertical axis plots the intensity [cts.] and the x-axis plots the angle values 2Θ [°]. The yellow curve shows the course of the measurement itself, the other curves are the result of peaks fitting and background and the pink curve shows proportion of amorphous phase.

Table 6: Percentage of crystalline and amorphous phase of MMT 30 B + TPU masterbatch

Phase Type	Area [cts. °]	Rel. Mass [%]
Crystalline	28,88	81,0%
Amorphous	6,75	19,0%

MMT 30 B itself contains a large proportion of the crystalline phase, 96,5 %. The first high peak is at a 2Θ angle of 4.83°, and the second very small and broad peak is around 20.00° (Fig. 14). For the masterbatch with this filler (Fig. 15), the first peak remains at an angle of 2.68°, and the second has broadened and is around 20.02°. A new peak has appeared at 5.39°. A more obvious leftward shift can be observed for the left and right peaks compared to the masterbatch with MMT 15 A. This shift and the appearance of a new peak, which is probably part of originally peak devided, again indicates intercalation of the filler, this time in a greater extent than in the previous filler.

6.1.7 GO2 (powder)

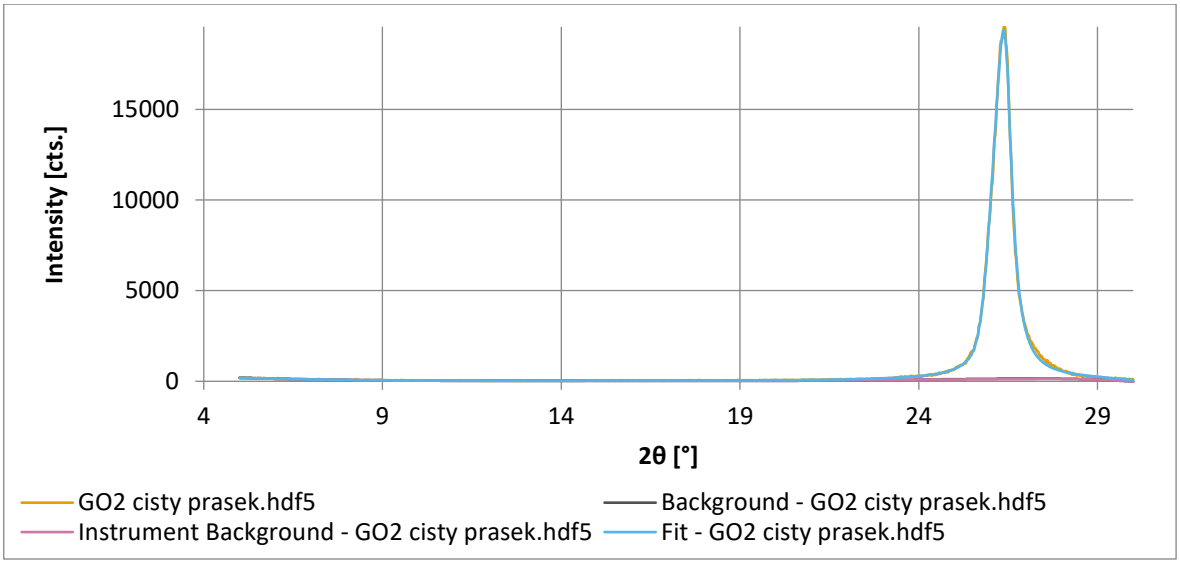

Figure 16: XRD measurement record for GO 2 powder, the vertical axis plots the intensity [cts.] and the x-axis plots the angle values 2Θ [°]. The yellow curve shows the course of the measurement itself, the other curves are the result of peaks fitting and background the pink curve shows proportion of amorphous phase.

Table 7: Percentage of crystalline and amorphous phase of GO 2 powder

Phase Type	Area [cts. °]	Rel. Mass [%]
Crystalline	294,74	99,5%
Amorphous	1,48	0,5%

6.1.8 GO2 + TPU 11T80

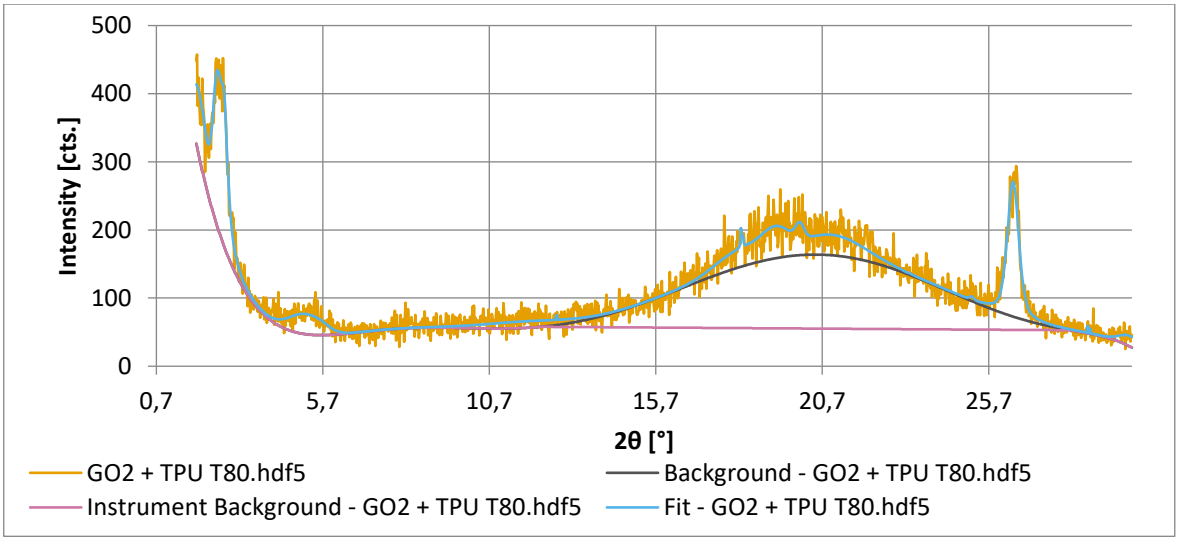

Figure 17: XRD measurement record for MMT 30 B + TPU masterbatch, the vertical axis plots the intensity [cts.] and the x-axis plots the angle values 2Θ [°]. The yellow curve shows the course of the measurement itself, the other curves are the result of peaks fitting and background, and the pink curve shows proportion of amorphous phase.

Table 8: Percentage of crystalline and amorphous phase of GO 2+ TPU masterbatch

Phase Type	Area [cts. °]	Rel. Mass [%]
Crystalline	6,19	28,1%
Amorphous	15,81	71,9%

In the graph (Fig. 16) only one peak is visible, and that for 2Θ 26.39°. For the filler mixed into the TPU matrix, a different behavior can be observed compared to the other fillers. In the graph (Fig. 17), the peaks corresponding to the GO filler 2, which is the peak at 26.41°, and to the pure TPU, a broad peak around 20.00°, can be seen. At lower angles, there are two peaks in the graph that do not correspond to either material. The first peak could correspond to the MMT 15 A filler, which may have accidentally entered the mixture during extrusion, even though the extruder was cleaned with pure TPU before each mixture change. Another, small peak would subsequently correspond to intercalated MMT 15 A. As for the peaks corresponding to the input materials, the peak corresponding to the GO 2 filler is not significantly shifted, it just got smaller, which is sign of exfoliation, the peak corresponding to the pure TPU is shifted towards lower angles by 1°, which is not considered a significant shift. The peak for TPU remained very high compared to the other blends, which also indicates insufficient filler incorporation.

A significant change has occurred in the proportion of crystalline phase. While GO 2 is more crystalline, TPU is minimally crystalline. The mixture of the two materials contains only 28.1 % crystalline phase, therefore it is mostly amorphous.

7 RHEOMETER

Anton Paar's Modular Compact Rheometer MCR 502 (Fig. 21) was used for oscillatory measurements to evaluate the dependence of Storage Modulus, Loss Factor and Complex Viscosity on Frequency and the dependence of Complex Shear Modulus, Loss Factor on Temperature. In general, this measurement will describe the properties of melt that are needed for further processing of the material. Storage and Complex Shear Modulus correspond to the material's response to deformation and determine the resistance to this deformation, similar to viscosity, which corresponds to the resistance of the liquid to deformation. The Loss Factor can be used to determine when the material behaviour corresponds to a solid (<1) or a liquid (>1).

Circular samples of 0.5 mm diameter for this measurement were die-cut from extruded masterbatch plates and pure TPUs types. The measurement conditions were as follows: the first interval (I1) had a constant temperature of 190 °C, in the second interval (I2) there was a cooling to 80 °C and a reheating to 190 °C in the third interval (I3), the fourth interval (I4) was again at a constant temperature of 190 °C.

Figure 18: Anton Paar's Modular Compact Rheometer MCR 502

7.1 Results and Discussion

7.1.1 Storage Modulus G´ vs. Frequency

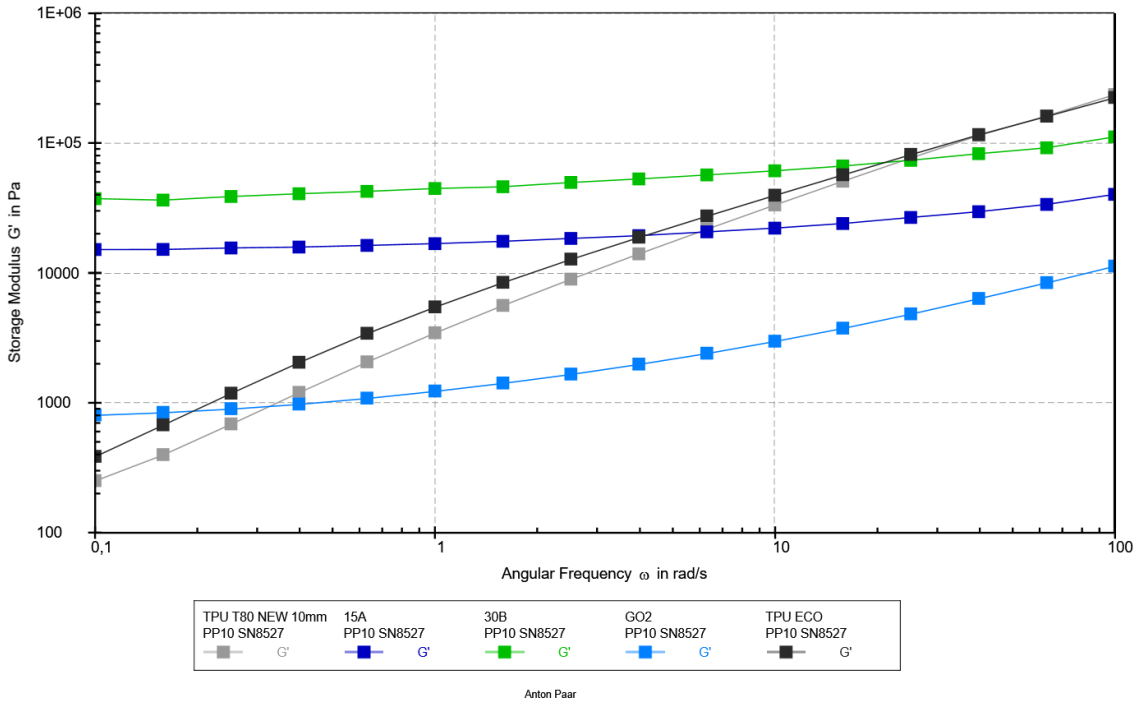

Figure 19: Dependence of Storage Modulus G´ [Pa] on frequency change [rad/s] for pure TPUs and TPU 11T80 nanocomposites with MMT fillers 15 A (20 wt.%) and 30 B (20 wt.%) and GO2 (10 wt.%).

From the curves in Fig. 19, it can be seen that the TPU types (black and grey curves) respond very similarly to deformation, with their resistance increasing significantly with increasing frequency. Nanocomposites with MMT 15 A and 30 B (green and dark blue curves) show a similar pattern, the initial value of Storage Modulus G′ is almost two orders of magnitude higher than for the pure material, and further there is no significant increase with increasing frequency. These fillers are able to stiffen the material, 30 B a little more. In contrast, the nanocomposite with GO2 starts at low frequencies at a G´ value close to the pure TPU 11T80, increasing with increasing frequency, but not as significantly as the pure material, thus the toughening was not significant.

7.1.2 Loss Factor tanδ vs. Frequency

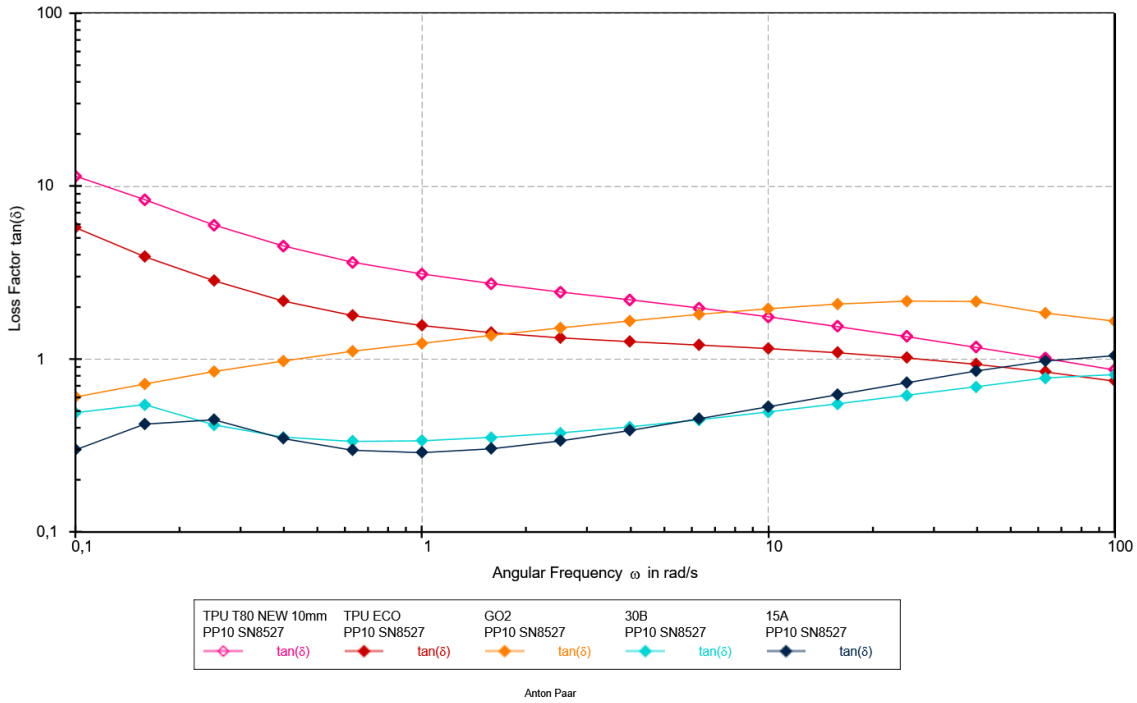

Figure 20: Dependence of Loss Factor tanδ on frequency change [rad/s] for pure TPUs and TPU 11T80 nanocomposites with MMT fillers 15 A (20 wt.%) and 30 B (20 wt.%) and GO2 (10 wt.%).

In the diagram of Fig. 20, it can be seen that both TPUs (pink and red curves) behave like liquids up to a frequency of about 80 rad/s, where their tanδ value drops below 1 and their behavior is more consistent with a solid. For the nanocomposites with MMT (black and blue curves), their stiffening function is confirmed here as they behave like solids throughout the measurement. There is no significant difference between the effect of the 15 A and 30 B fillers, only the material with the 30 B filler holds even at a maximum frequency below 1, so its reinforcement is slightly more effective than that of the 15 A. The nanocomposite with GO2 filler (orange curve) behaves like a solid only at low frequencies, then rises before 1 rad/s and behaves like a liquid up to a final frequency of 100 rad/s. Reinforcement with this filler has not really happened.

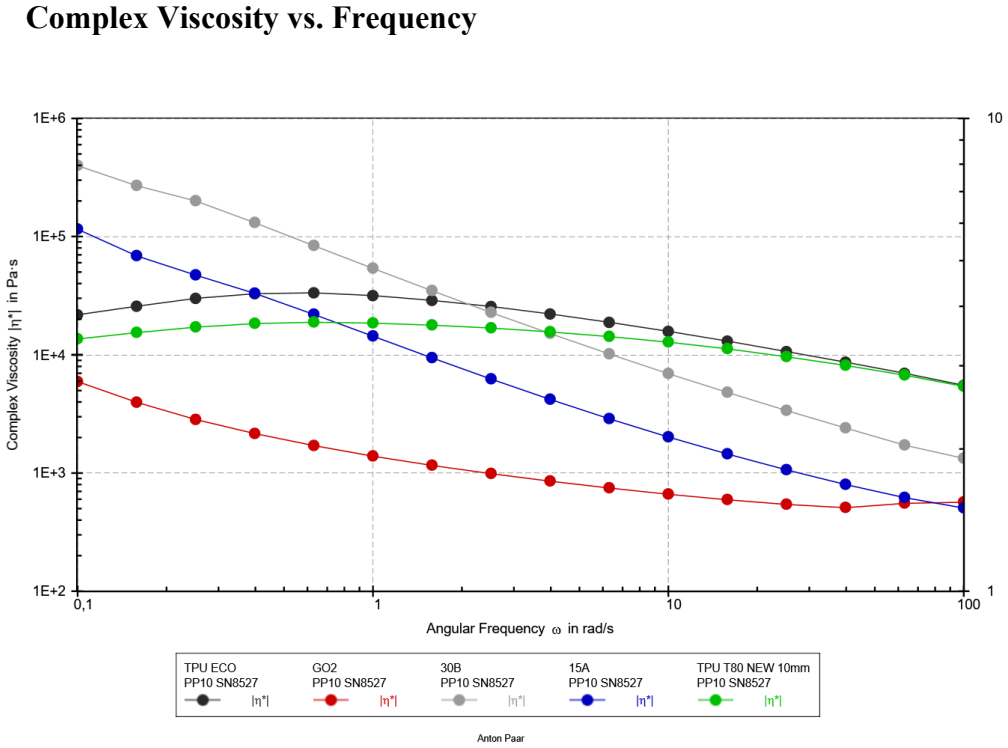

Figure 21: Dependence of Complex Viscosity [Pa.s] on frequency change [rad/s] for pure TPUs and TPU 11T80 nanocomposites with MMT fillers 15 A (20 wt.%) and 30 B (20 wt.%), and GO2 (10 wt.%); the sample was tested immediately after pressing..

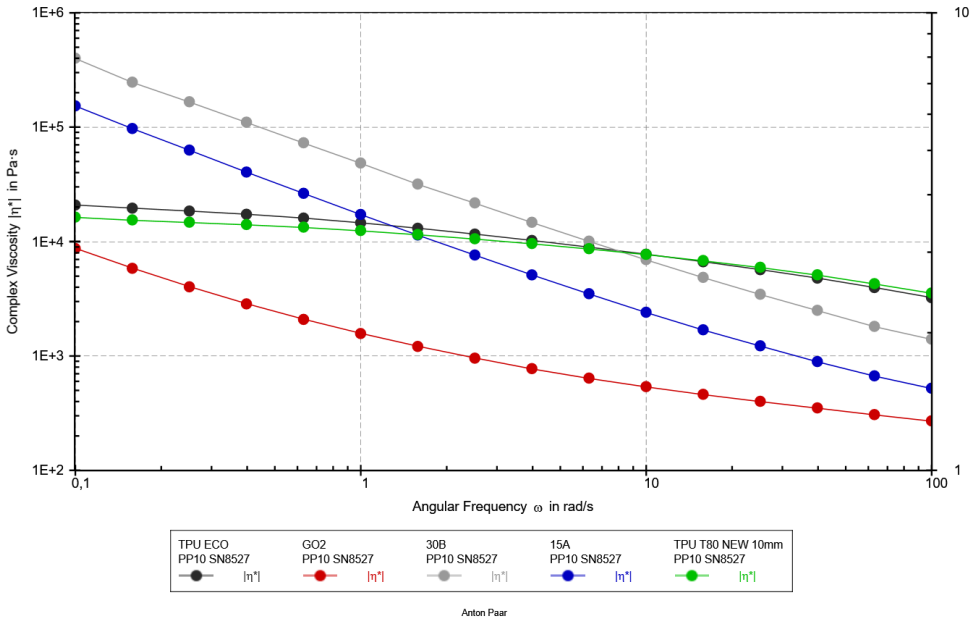

Figure 22: Dependence of Complex viscosity [Pa.s] on frequency change [rad/s] for pure TPUs and TPU 11T80 nanocomposites with MMT fillers 15 A (20 wt.%) and 30 B (20 wt.%), and GO2 (10 wt.%), this measurement was made on the same specimen as the previous one, but meanwhile it was cooled and reheated and went through deformation.

The graph (Fig. 21) shows the viscosity versus frequency. Both types of TPU behave similarly, with TPU ECO having only slightly higher viscosity. The TPU 11T80 filled MMT types have the very highest viscosities at low frequencies, but these drop sharply with increasing frequency to below the values of the TPU types. The blend with GO 2 filler has the lowest viscosity of all the measured blends at the lowest frequency, and the viscosity drops only slightly thereafter.

The curves in the second graph (Fig. 22), which shows the same dependence but after cooling and reheating the material, can be compared with the first graph. After erasing the thermal history, the two types of TPU started to behave almost identically. Their waveform at lower frequencies doesn't grow as much and again the curves drop almost linearly. For MMT fillers, the curves did not change significantly. The TPU with GO 2 filler has a slightly higher viscosity at lower frequencies and decreases noticeably more with increasing frequency.

7.1.3 Complex Shear Modulus G* vs. Temperature

The following graphs show the cooling (I2) and heating (I3) curves.

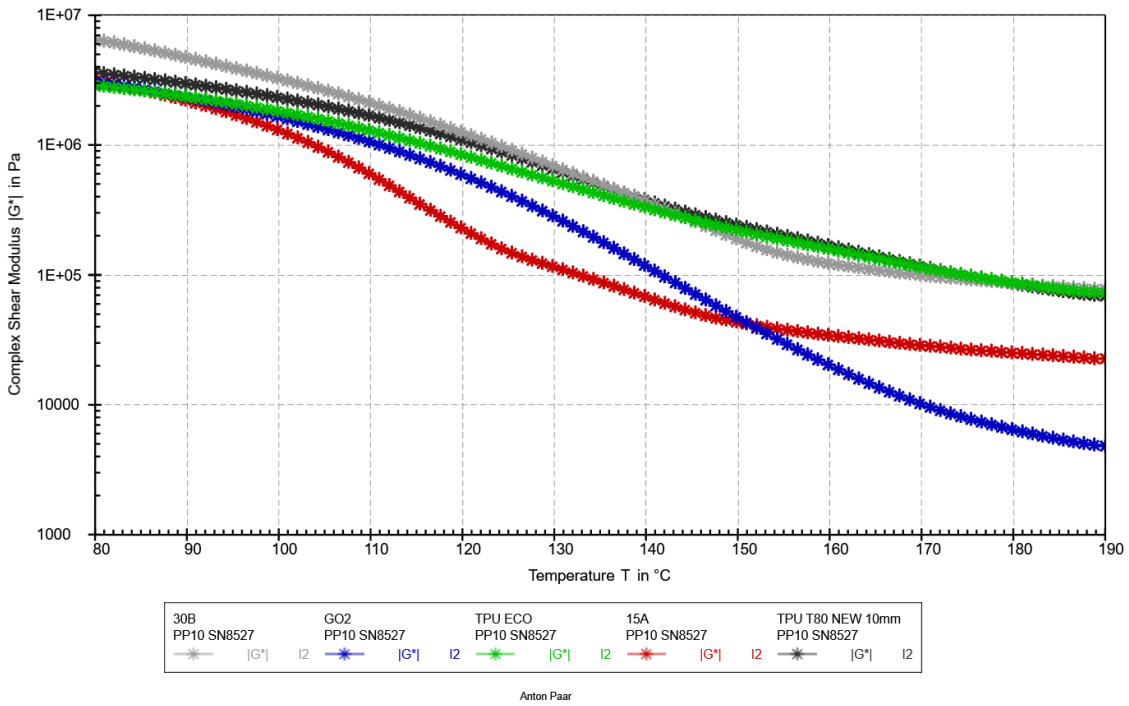

Figure 23: Dependence of Complex Shear Modulus G* [Pa] on temperature [°C] for pure TPUs and TPU 11T80 nanocomposites with MMT fillers 15 A (20 wt.%) and 30 B (20 wt.%) and GO2 (10 wt.%). (Cooling 190-80°C)

The Complex Shear Modulus shown in Fig. 23 corresponds to the response of the material to the ongoing deformation. This measurement was made while cooling the melt from 190 °C to 80 °C. TPU ECO and TPU 11T80 (green and black curves) again have a similar waveform, the Complex Shear Modulus G* for TPU 11T80 ends at a higher value at the lowest temperature. Both TPUs increase their resistance to deformation with decreasing temperature. The blend with GO2 (blue curve) is at much lower values than the pure TPU during the measurement. In this graph, the MMT 15 A filler (red curve) does not show good stiffening either, as its G* values are much lower in the waveform than the values for the pure materials and the nanocomposite with 30 B (grey curve). However, all the measured materials, except the nanocomposite with MMT 30 B, end up with approximately the same G* value at 80 °C, while 30 B rises above the other curves around 130 °C, continues to rise and reaches the highest G* value at the final temperature of 80 °C.

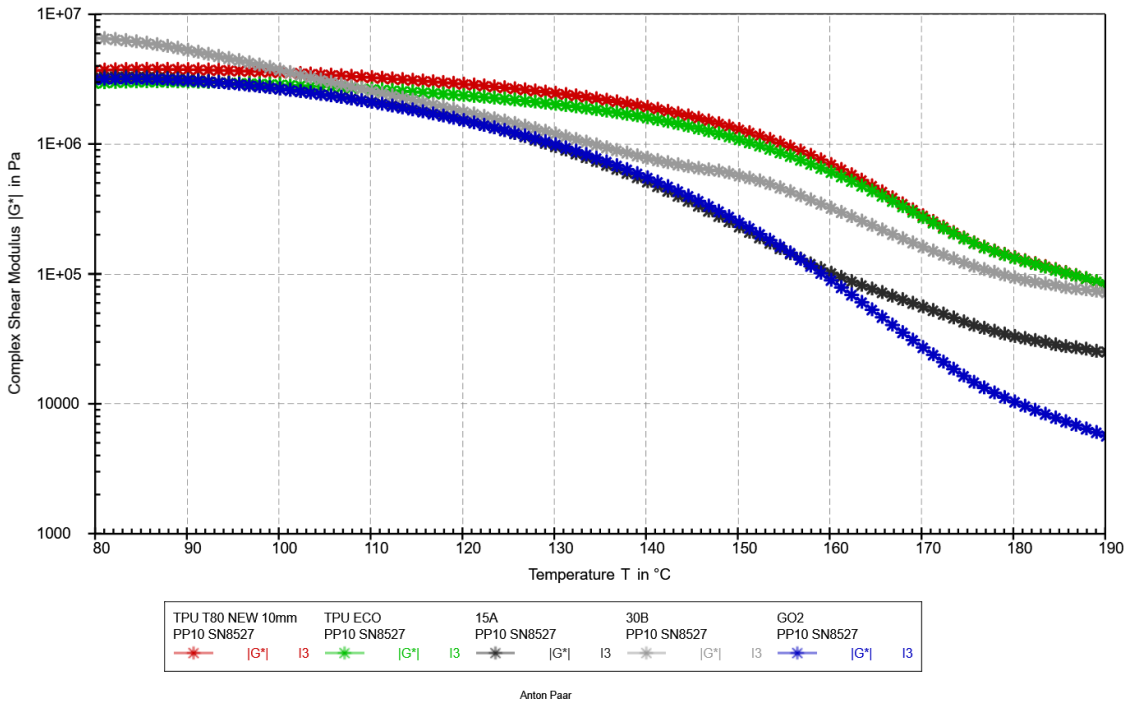

Figure 24: Dependence of Complex Shear Modulus G* [Pa] on temperature [°C] for pure TPUs and TPU 11T80 nanocomposites with MMT fillers 15 A (20 wt.%) and 30 B (20 wt.%) and GO2 (10 wt.%). (Heating 80-190°C)

The heating behavior of G* (Fig. 24), when heated back to 190 °C, is quite similar to cooling. The TPU types (red and green curves) behave very similarly, even overlapping at higher temperatures. For the nanocomposite with MMT 30 B filler (grey curve), the behaviour changes, starting at the highest values, but after 100 °C it drops below the TPUs curves and

stays at lower values. The mixtures with GO2 and MMT 15 A fillers (blue and black curves) have the same behaviour up to 160 °C, both start at the lowest G* values, slowly decrease and at 160 °C the curve for TPU+GO2 separates and drops more steeply than for the 15 A mixture.

After these two measurements (Figs. 23 and 24), the MMT 15A filler does not appear to be good, and after cooling and reheating, even the MMT B 30 filler did not show a stiffening effect. It is possible that these fillers degraded during the measurements and their effect was reduced/disappeared.

7.1.4 Loss Factor tanδ vs. Temperature

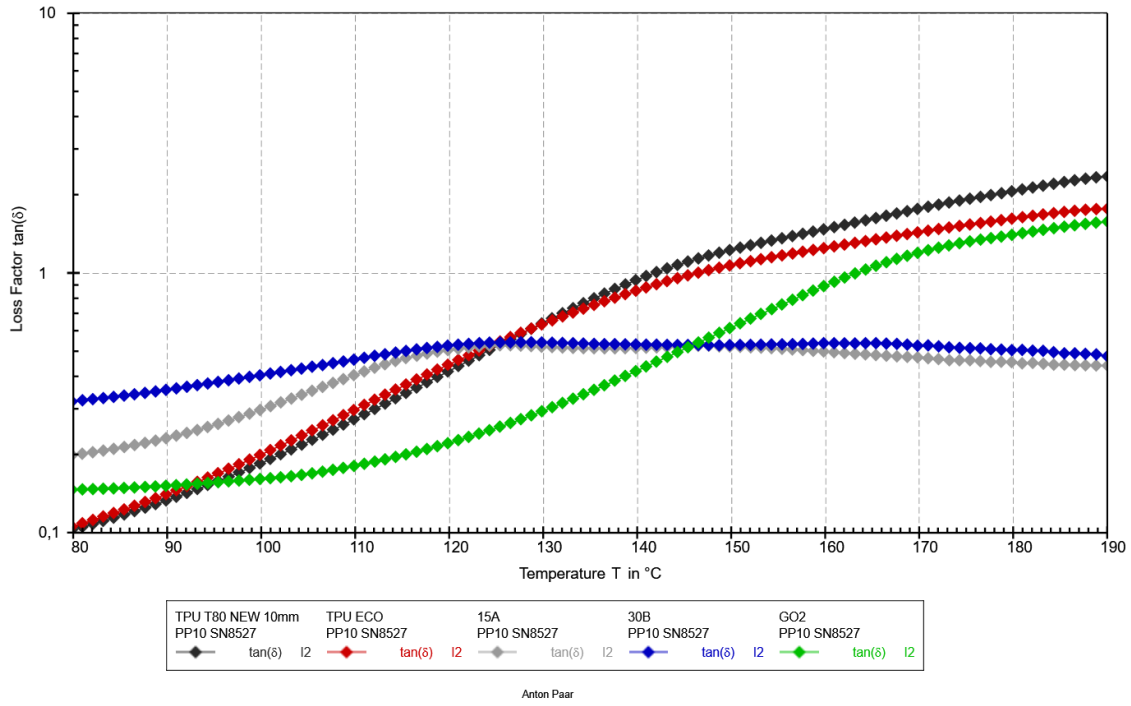

Figure 25:Dependence of Loss Factor tanδ on temperature [°C] for pure TPUs and TPU 11T80 nanocomposites with MMT fillers 15 A (20 wt.%) and 30 B (20 wt.%) and GO2 (10 wt.%). (Cooling 190-80 °C)

Fig. 25 shows the tanδ curve when cooling from 190 °C to 80 °C. The tan d for TPUs (black and red curves) again have a similar shape. They retain their liquid-like behaviour up to 140 °C and behave like solids at lower temperatures. The nanocomposites with MMT 15 A and 30 B (grey and blue curves) stay below 1 throughout the whole run and therefore behave like solids. The blend with GO2 (green curve) starts above 1 at higher

temperatures, but around 160 °C it exceeds the threshold of value tanδ 1 and behaves as a solid, even taking on lower values than the other two fillers at lower temperatures.

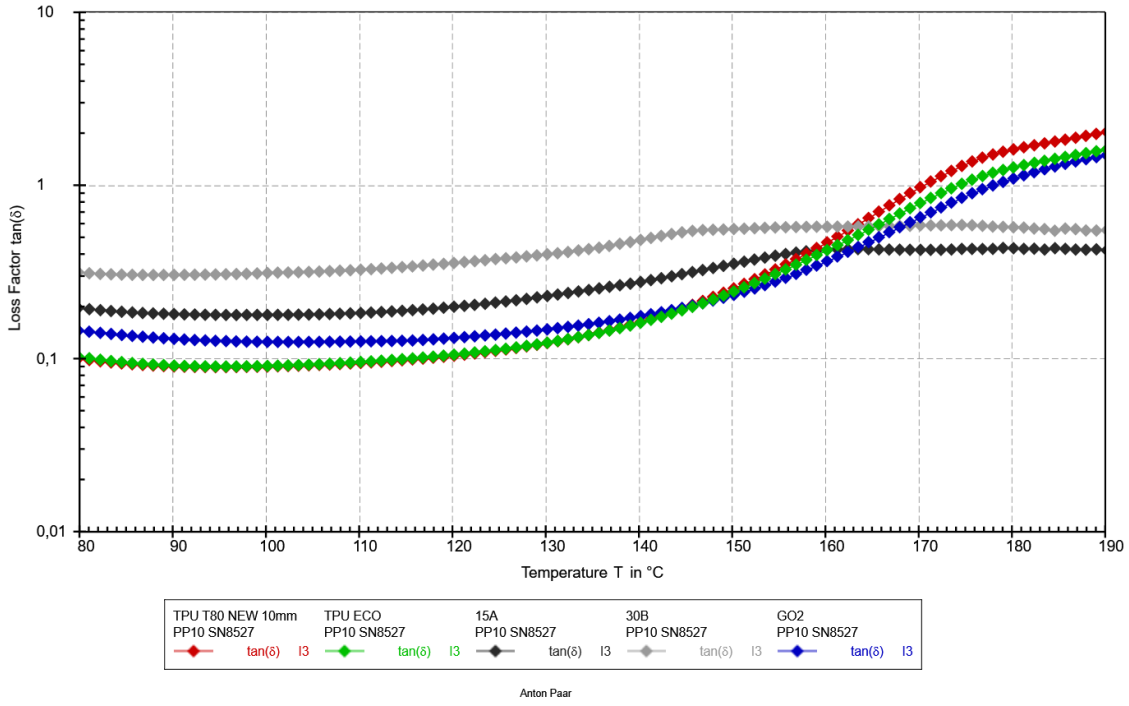

Figure 26: Dependence of Loss Factor tanδ on temperature [°C] for pure TPUs and TPU 11T80 nanocomposites with MMT fillers 15 A (20 wt.%) and 30 B (20 wt.%) and GO2 (10 wt.%). (Heating 80-190 °C)

On reheating (Fig. 26), the TPUs (red and green curves) changed their behaviour, staying very low below 1 until temperature 130 °C, starting to grow at 140 °C and exceeding the value of 1, at which point their behaviour changes to that of liquids, at around 175 °C. The nanocomposite with GO2 (blue curve) behaves very similarly to the polymer matrix and its behavior has also changed. During cooling it did not get above 1 and stayed below this value for the whole measurement, here it stays below this value and crosses it around 180 °C. The nanocomposites with MMT 15 A and 30 B fillers (black and grey curves) have a very similar behaviour to that observed during cooling (Fig. 25).

8 DSC

This measurement was made to form an idea of the melting and crystallization temperature of the pure and filled material. The measurements were performed on the DSC 1 STAR^e System from METTLER TOLEDO (Fig. 34). The samples were extruded materials, thus pure TPU 11T80 and TPU ECO D12T80E, and filled TPU 11T80 with MMT 30 B (20 wt.%), MMT 15 A (20 wt.%) and GO2 (10 wt.%). The sample weights were 4.24 g 30 B, 3.55 g 15 A, 3.89 g GO2, 3.57 g TPU 11T80 and 3.68 g TPU ECO D12T80E. The measurements were carried out in an inert atmosphere (N2) and the temperature changes were as follows: from 25 °C at 20 K/min to 220 °C, then at 10 K/min to 5 °C and back to 220 °C at the same rate, finally the temperature was reduced to 25 °C at 20 K/min.

The instrument evaluated the measurements as a plot of heat capacity versus temperature and the melting and crystallization temperatures could be read from the peaks on the first cooling and second heating curves.

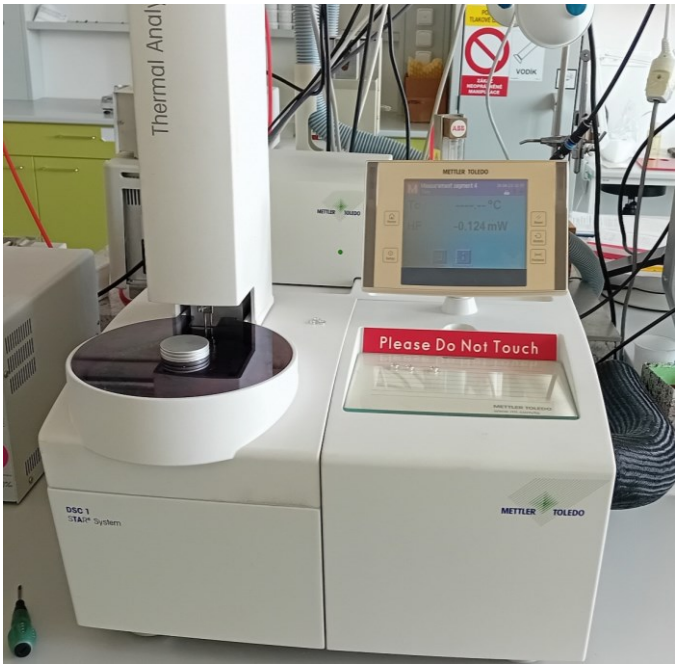

Figure 27: DSC 1 by Mettler Toledo

8.1 Results and Discussion

8.1.1 TPU 11T80

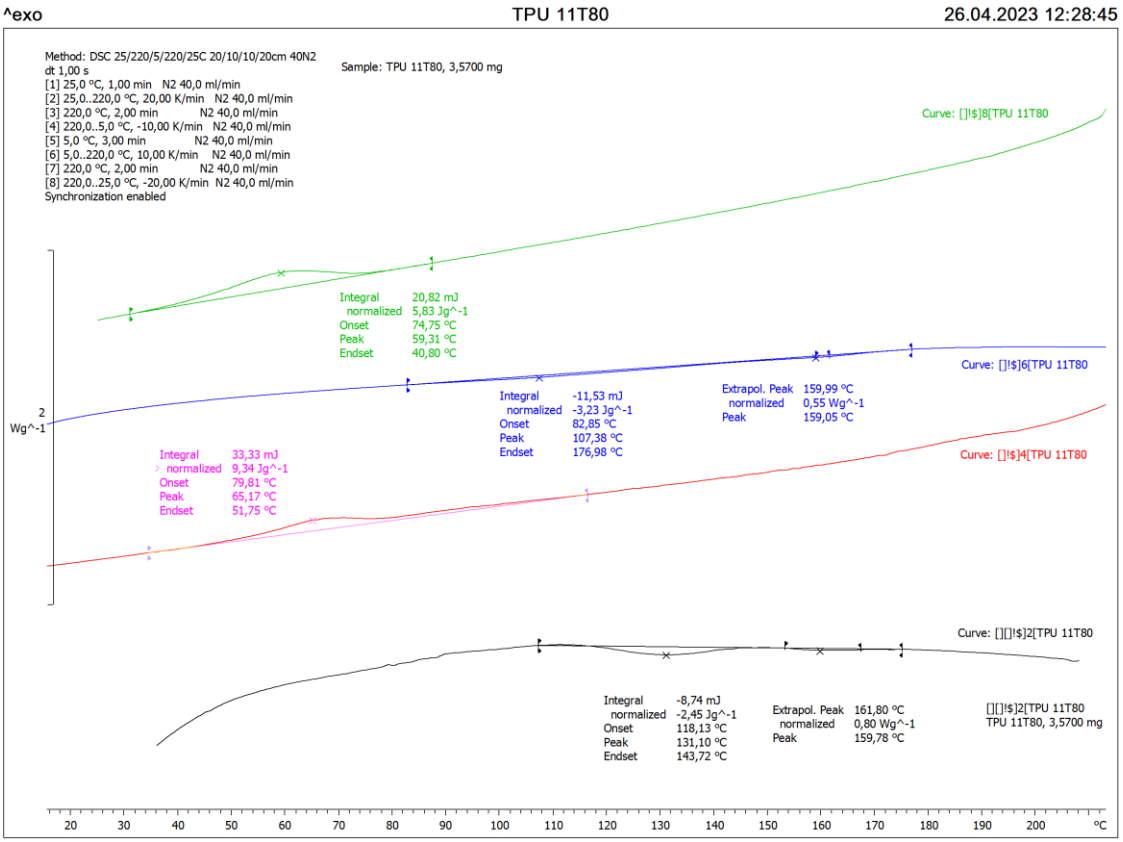

Figure 28: DSC measurement record for pure TPU 11T80

From the red curve of the first cooling, the crystallization temperature was determined to be 65.17 °C; the blue curve of the second heating shows two peaks, one at 159.05 °C and the other at 107.38 °C. These peaks correspond to the melting temperature, while at the lower temperature most of the crystalline phase may have melted and at the second temperature the rest of this phase melted. Since the peaks are not as significant, we can assume that the material is poorly crystalline because not as much of the supplied energy was used for melting and crystallization.

8.1.2 TPU ECO D12T80E

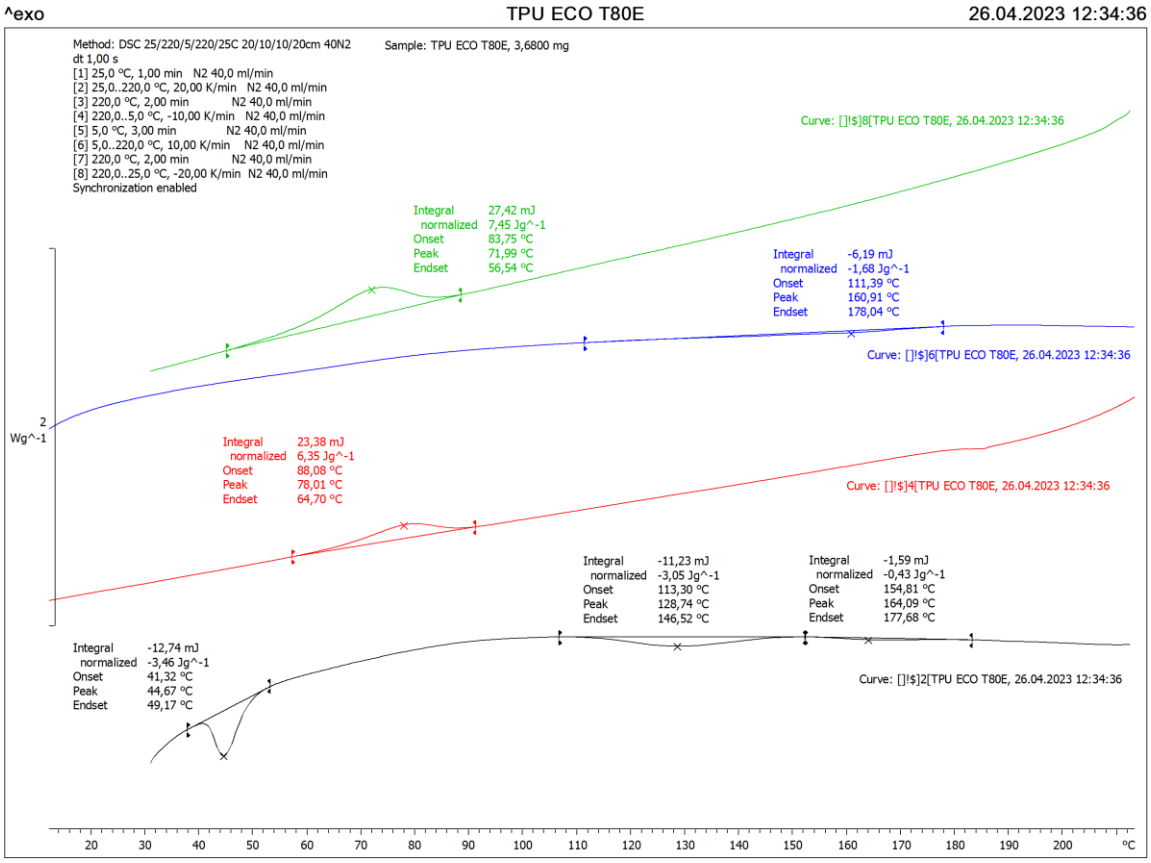

Figure 29: DSC measurement record for pure TPU ECO D12T80E

The crystallization temperature for this material was determined to be 78.01 °C, this peak is more pronounced than for the other TPU, it is possible that more material has crystallized, thus a higher crystallinity of this type could be observed compared to the previous TPU. The melting temperature was evaluated at 160.91 °C, which could be compared to the value of the second peak for TPU 11T80.

8.1.3 TPU 11T80 + MMT 15 A

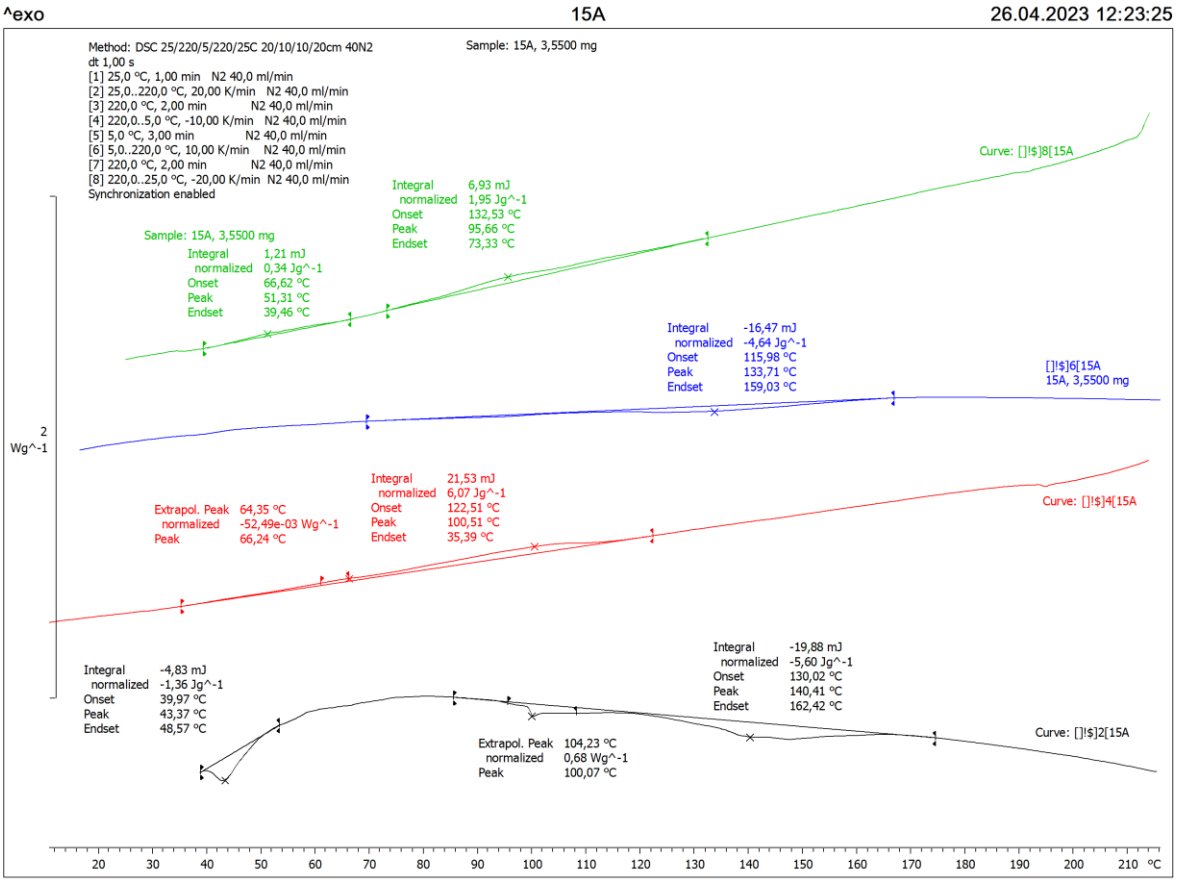

Figure 30: DSC measurement record for MMT 15 A

From this graph we can observe the differences of the filled TPU 11T80 with MMT 15 A filler from pure TPU. As for the crystallization temperature, the curve showed two peaks, one with a value of 66.24 °C and the other 100.51 °C.

The melting temperature for pure TPU was evaluated for two peaks, there is only one peak on this curve for the filled material corresponding to 133.71 °C. This value lies between the values evaluated for pure TPU. With a more detailed evaluation, it would probably be possible to evaluate one more peak at a lower temperature, around 90 °C. Consequently, it could be concluded that the filler has lowered the melting temperature.

8.1.4 TPU 11T80 + MMT 30 B

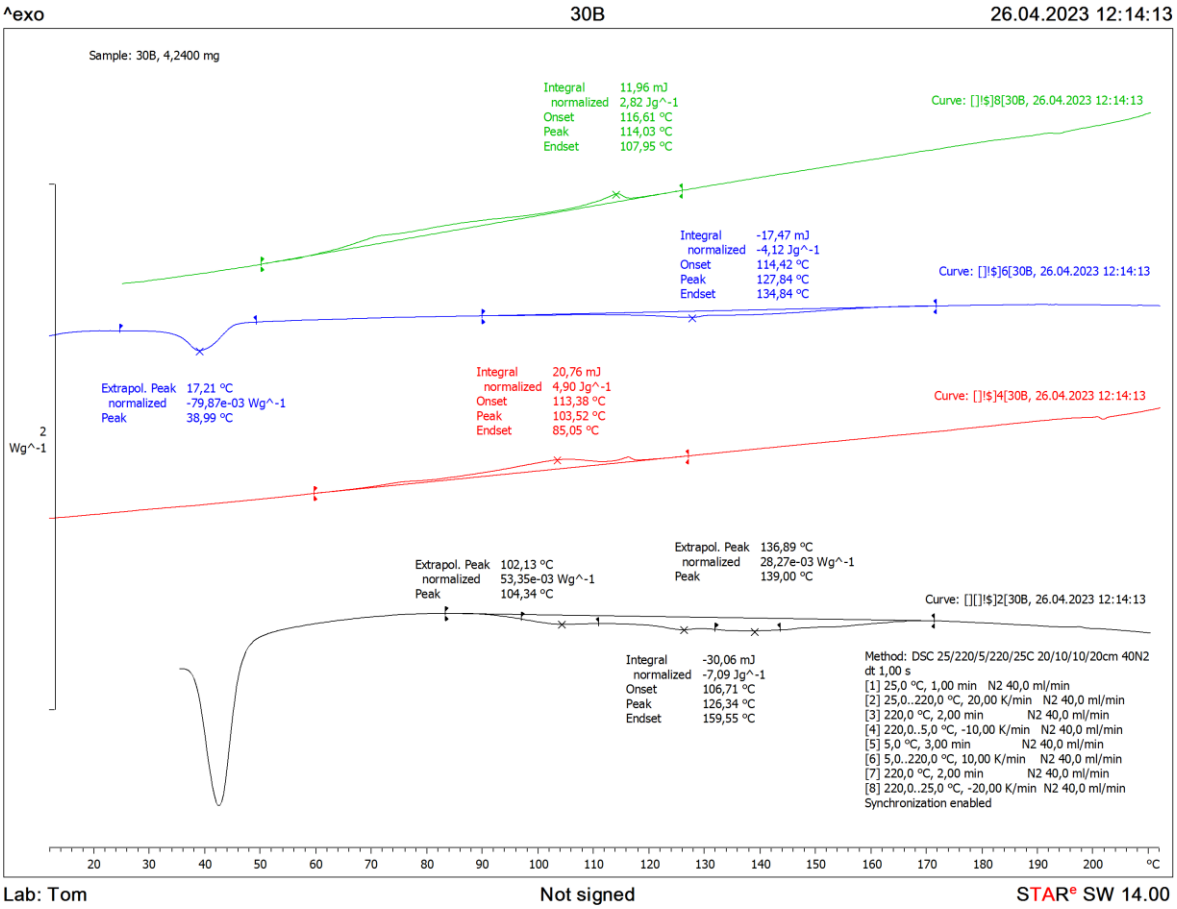

Figure 31: DSC measurement record for MMT 30 B

For the mixture of TPU and MMT 30 B, the first cooling curve shows a peak of 103.52 °C. This temperature is very far from the crystallization temperature of pure TPU. There is a slight peak before this peak, which corresponds to a value of approximately 70 °C, which would match the crystallisation temperature of pure TPU. The peak evaluated would therefore indicate the crystallisation temperature of the filler.

In the second heating curve, a peak at 38.99 °C can be seen, which is well below the melting temperature of pure TPU and does not correspond to the crystallization temperature of the mixture. The second peak with a top at 127.84 °C is again between the peak values of the pure TPU curves. It is possible that the structure of the filler forms and holds the amorphous portion of the matrix, thus providing the physical crosslinking itself and not allowing the TPU to crystallize as much. This would explain the very small peak with a temperature value corresponding to the crystallization temperature of pure TPU.

8.1.5 TPU 11T80 + GO2

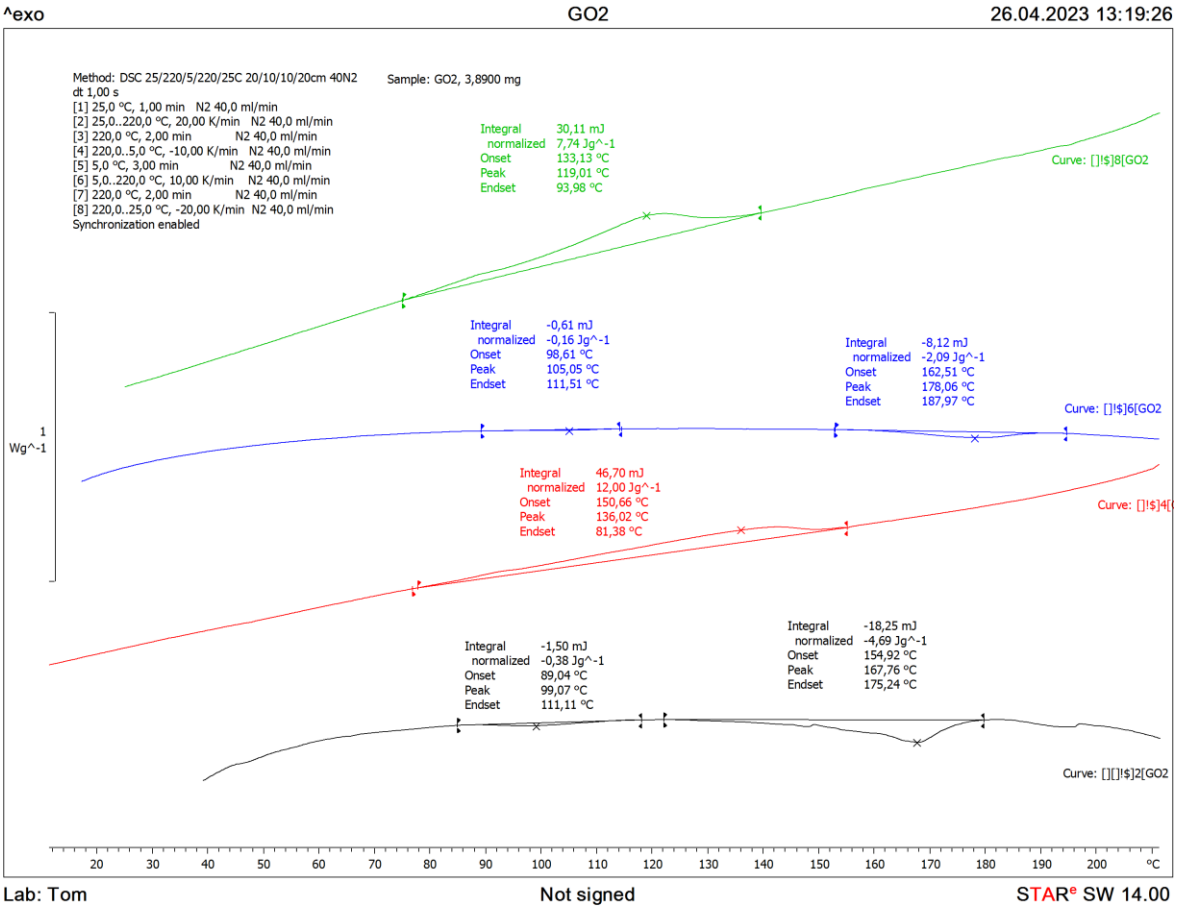

Figure 32: DSC measurement record for GO2

From the first cooling curve, a crystallization temperature of 136.02 °C can be read. This peak is the only one visible on the curve and the evaluated value differs significantly from the crystallization temperature of pure TPU, it is reasonable to consider the evaluated value as the crystallization temperature shifted because of the addition of filler. It is possible that the crystallization of the filler has covered the crystallization of the matrix itself. The phase transition of the matrix was observed on the second heating curve.

The melting temperatures were evaluated at 105.05 °C and 178.06 °C. The first value corresponds to the lower value found for the pure material. The second value evaluated is significantly higher than the second temperature found for pure TPU, so it is most likely the melting temperature of the filler.

9 DMA

This method was used to evaluate the glass transition temperature for clean and filled materials.

Samples used for this measurement were overflows from moulded plates of half millimetre thickness. These plates were further used for rheological measurements. The thicknesses of the plates ranged from 30 to 60 µm. Length of the test area was always 10 mm. Samples were deformed in tension. The measurements were performed on a METTLER TOLEDO DMA 1 (Fig. 40) with the STAR System evaluation program.

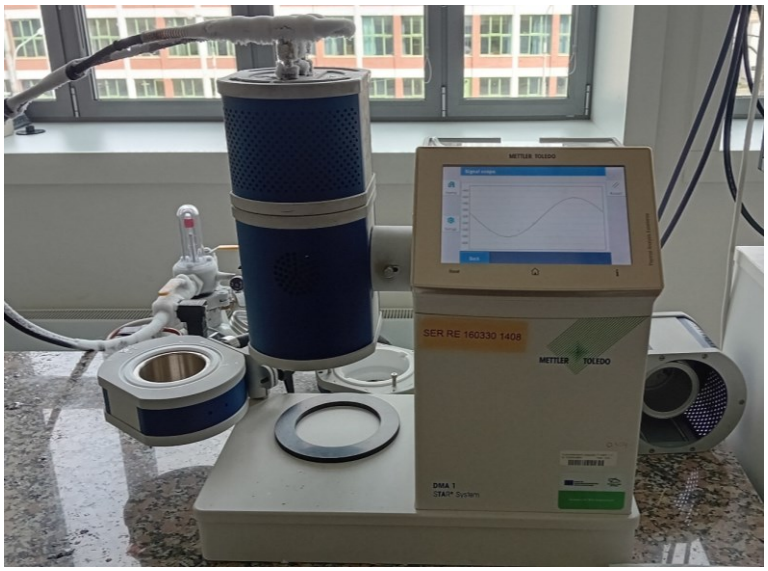

Figure 33: DMA 1 by Mettler Toledo

9.1 Results and Discussion

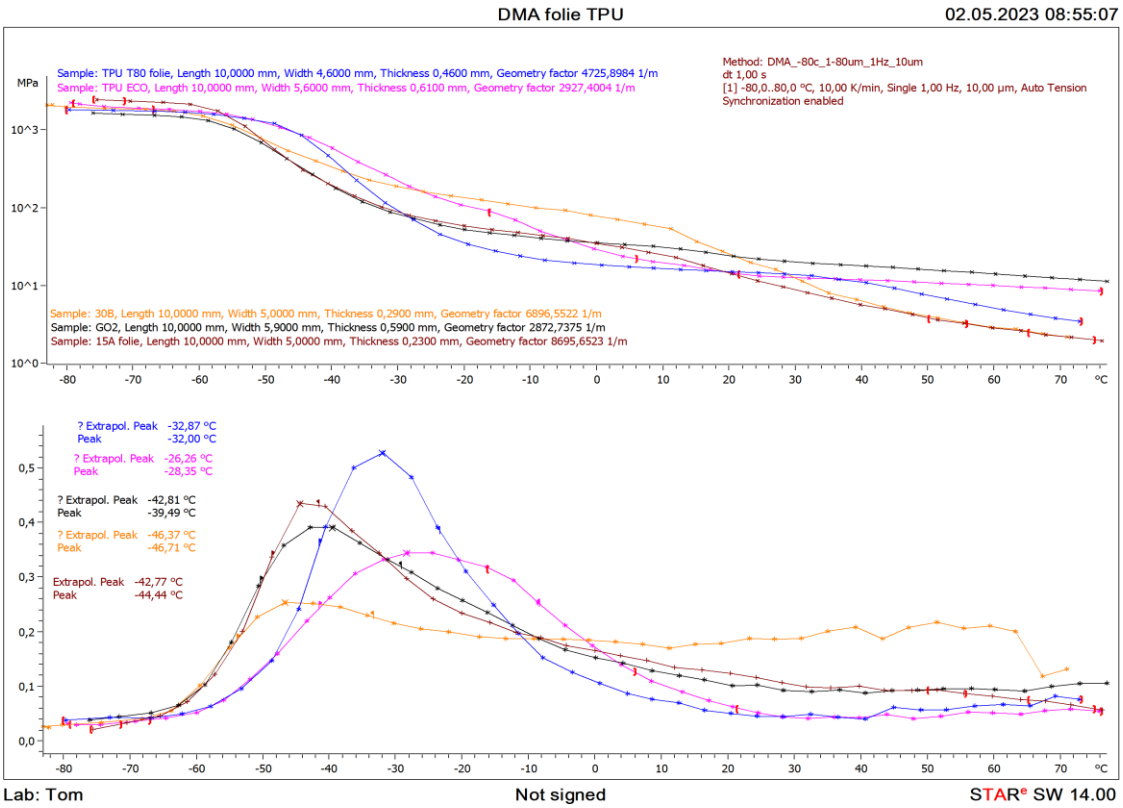

Figure 34: DMA results for all materials, top graph: dependence of E´ modulus on temperature, bottom graph: dependence of tanδ on temperature

Using the DMA method, the glass transition temperatures for pure and filled materials were determined. From the top graph, which shows the dependence of the E' modulus on temperature, it is evident that the filler MMT 30 B stiffens the material temperatures up to 10 °C, as its curve is higher than the others, subsequently drops below TPUs (pink and blue curves) and the mixture with GO2 (black curve). The lower the modulus with temperature, the lower the resistance to deformation of the material. The addition of fillers reinforces the flexible component of the material and therefore makes it more resistant to deformation.

The lower graph, representing the relation of tanδ to temperature, shows that the peaks of the curves for filled materials shift to the left towards lower temperatures, which again indicates a stiffening of the material. For pure TPU 11T80, from which the masterbatches were formed, the glass transition temperature (T_g) was - 32.00 °C, for TPU ECO D12T80E T_g = - 28.35 °C. The GO2 filled material had a T_g of - 39.49 °C. The other two MMT blends showed similar glass transition temperatures, respectively - 46.71 °C for MMT 30 B and - 44.44 °C for MMT 15 A.

10 GTR TESTING

The measurements were carried out on the VAC - V1 instrument from Labthink® (Fig. 18). Samples for gas permeability measurements, specifically for technical air permeability, were made from blown films. The evacuation of both chambers took 1.5 h. For each sample, the thickness was measured five times and their average was put into the measuring program, the test area of all samples was the same, that is 38.48 cm^2.

Figure 35: VAC - V1 Labthink®

10.1 Results and Discussion

First the results of the measurement of the parameter *GTR*, unit cm^3/m^2.day.0,1MPa, followed by the permeability factor *P*, unit Barrer, are inserted. The intermediate results are summarized in a table together with the average of the values, the figures show a graphical representation of these average values with error bars.

Table 9: Measured and average values of the GTR parameter

	GTR [cm^3/m^2.day.0,1MPa]			
	TPU	15A	30B 5 %	30B 10 %
	1667	2941	1678	2175
	1510	3644	1563	2776
	1517	2928	2164	2281
	1771	2055	1981	1566
(average ± deviation)	**(1 620 ± 70)**	**(2 900 ± 500)**	**(1 800 ± 200)**	**(2 200 ± 400)**

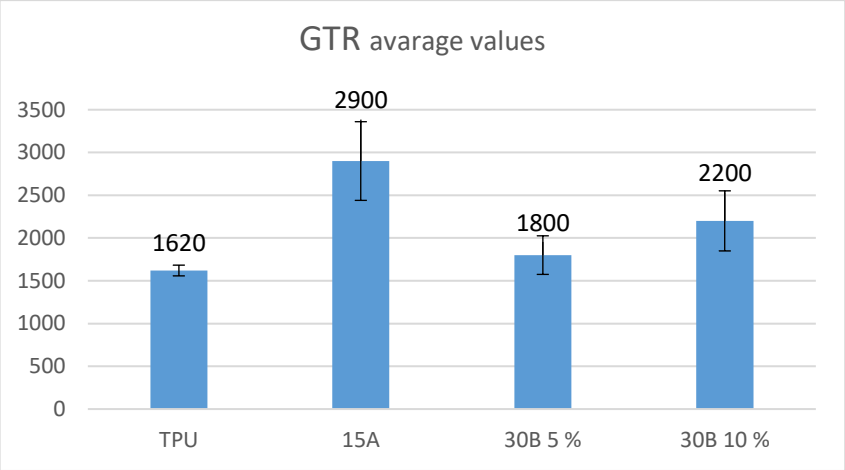

Figure 36: Average GTR values [cm^3/m^2.day.0.1MPa] for pure TPU and TPU nanocomposites with MMT fillers 15 A (5 wt.%) and 30 B (5 and 10 wt.%).

Table 10: Measured and average values of the permeability parametr *P*

	***P* [Barrer]**			
	TPU	15A	30B 5 %	30B 10 %
	1,632	1,074	1,737	0,828
	1,305	1,609	1,333	1,733
	1,346	1,429	1,663	1,893
	1,302	1,627	1,547	1,490
(average ± deviation)	**(1,40 ± 0,10)**	**(1,43 ± 0,19)**	**(1,57 ± 0,13)**	**(1,5 ± 0,4)**

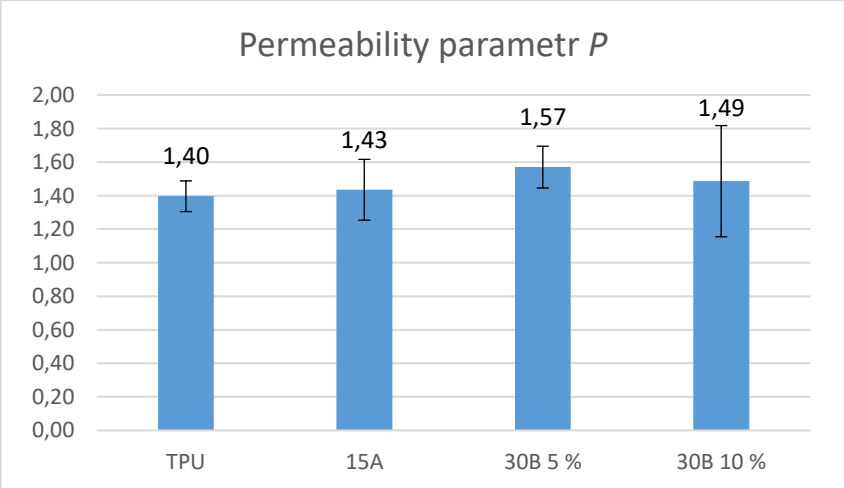

Figure 37: Average of permeability parametr *P* values [Barrer] for pure TPU and TPU nanocomposites with MMT fillers 15 A (5 wt.%) and 30 B (5 and 10 wt.%).

The measurement of gas permeability was essential for our experiment; other methods clarified other parameters or explained the results of this method.

From the measured GTR (gas transmission rate), we do not observe any improvement in the barrier properties of the filled materials compared to the bare matrix. If there was a significant change, our expectation was that this parameter would decrease by more than a thousand units. In all cases, an increase in this parameter can be seen, which may be due to uneven dispersion of the filler in the matrix or little adhesion of the filler to the matrix. These defects may have caused the formation of weaker spots that let air through with less resistance, and since this parameter is not affected by the thickness of the sample, the values may have been higher than for the original plain material.

The parameter P comes out differently than GTR due to the fact that it is converted over the sample thickness. The foils were not the same thickness in all places, in some parts the difference in thickness was as much as 20 μm. The differences in sample thicknesses could have been due to improper dispersion of masterbatch into the plain material. As a result, the average parameter values for the different fillers and pure TPU came out similarly and there was no significant change in permeability.

CONCLUSION

Based on literature research, available materials and processing methods, two types of montmorillonite and two types of graphene oxide were selected as modifying nanofillers for polyurethane type of thermoplastic elastomer.

Suitable mixing conditions were not found for the first type of graphene oxide, while the second type was successfully mixed into the matrix but was not evenly dispersed during blowing, therefore the films for gas permeation testing could not be blown. Pure TPU and three masterbatches: MMT 15 A at a concentration of 5 wt.% and MMT 30 B at concentrations of 5 and 10 wt.%, were tested on DSC and WAXD, in which the pure fillers were also tested. For rheological testing and DMA, plates were pressed from masterbatches and pure TPUs. Gas permeability testing was evaluated on blown films employing differential pressure method.

X-ray analysis showed slight intercalation of nanoclay fillers and exfoliation of GO2 in the polymer matrix. The rheological measurements showed the clay nanofillers to be good reinforcers, while GO2 did not reinforce the matrix. According to the DSC, the addition of fillers had an effect on the crystallization and melting temperature. The DMA results showed a shift of the glass transition temperature towards lower values and good reinforcing properties of the MMT 30 B filler, but only up to a temperature of around 10 °C.

An improvement in barrier properties was expected for the modified material, which did not occur. This is probably due to the achieved intercalation of nanoparticles used in the polymer matrix nevertheless not their exfoliation. The only filler that was exfoliated was GO2, which, however, could not be blown out into films for measurements due to the significant change of viscosity properties of employed thermoplastic elastomer matrix. It is very possible that this filler would have guaranteed the expected decrease of gas permeability.

To further test the barrier properties, it would be good to try other methods of incorporating the filler that were mentioned in the research, such as mixing the nanofiller and polymer in solution.

BIBLIOGRAPHY

[1] BIRON, Michel. Basic Criteria for the Selection of Thermoplastics. In: *Thermoplastics and Thermoplastic Composites* [online]. B.m.: Elsevier, 2018, s. 133–202. Dostupné z: doi:10.1016/b978-0-08-102501-7.00003-5

[2] RALLINI, M. a José M. KENNY. Nanofillers in Polymers. In: *Modification of Polymer Properties* [online]. B.m.: Elsevier Inc., 2017, s. 47–86. ISBN 9780323443982. Dostupné z: doi:10.1016/B978-0-323-44353-1.00003-8

[3] MCKEEN, W. Laurence. *Permeability Properties of Plastics and Elastomers*. 2017.

[4] SIRACUSA, Valentina, Jean PINSON a Damien THIRY. *Surface Modification of Polymers for Food Science 12.1 Introduction*. 2020.

[5] OZBAS, Bulent, Christopher D. O'NEILL, Richard A. REGISTER, Ilhan A. AKSAY, Robert K. PRUD'HOMME a Douglas H. ADAMSON. Multifunctional elastomer nanocomposites with functionalized graphene single sheets. *Journal of Polymer Science, Part B: Polymer Physics* [online]. 2012, **50**(13), 910–916. ISSN 08876266. Dostupné z: doi:10.1002/polb.23080

[6] *https://www.engplastics.com.au/what-is-elastomer-and-its-uses/*. 30. květen 2014.

[7] KUMAR, Sudheer, Sukhila KRISHNAN a Smita MOHANTY. Applications of elastomer blends and composites. In: *Elastomer Blends and Composites* [online]. B.m.: Elsevier, 2022, s. 305–329. Dostupné z: doi:10.1016/B978-0-323-85832-8.00003-1

[8] DICK, John S. Rubber Technology - Compounding and Testing for Performance (3rd Edition). 2020.

[9] HUANG, Rongzhi, Priyakrit CHARI, Jung Kai TSENG, Guojun ZHANG, Mark COX a Joao M. MAIA. Microconfinement effect on gas barrier and mechanical properties of multilayer rigid/soft thermoplastic polyurethane films. *Journal of Applied Polymer Science* [online]. 2015, **132**(18). ISSN 10974628. Dostupné z: doi:10.1002/app.41849

[10] ALEXANDRE, Michael a Philippe DUBOIS. Polymer-layered silicate nanocomposites: preparation, properties and uses of a new class of materials. *Materials Science and Engineering: R: Reports* [online]. 2000, **28**(1–2), 1–63 [vid. 2023-05-16]. ISSN 0927-796X. Dostupné z: doi:10.1016/S0927-796X(00)00012-7

[11] SONG, Sung Ho. Synergistic Effect of Clay Platelets and Carbon Nanotubes in Styrene-Butadiene Rubber Nanocomposites. *Macromolecular Chemistry and Physics* [online]. 2016, **217**(23), 2617–2625. ISSN 10221352. Dostupné z: doi:10.1002/macp.201600344

[12] HUANG, Zhibo, Xiaohui WU, Yan SHI a Liqun ZHANG. A Novel Interface Agent for Preparation of High Gas Barrier Organic Montmorillonite/Brominated Butyl Rubber Nanocomposites. *Macromolecular Materials and Engineering* [online]. 2022. ISSN 14392054. Dostupné z: doi:10.1002/mame.202200567

[13] SARITHA, Appukuttan a Kuruvilla JOSEPH. Role of solvent interaction parameters in tailoring the properties of chlorobutyl rubber nanocomposites. *Polymer Composites* [online]. 2016, **37**(2), 353–359. ISSN 15480569. Dostupné z: doi:10.1002/pc.23187

[14] QIAN, Yuqiang, Wenhao LIU, Yong Tae PARK, Chris I. LINDSAY, Rafael CAMARGO, Christopher W. MACOSKO a Andreas STEIN. Modification with tertiary amine catalysts improves vermiculite dispersion in polyurethane via in situ intercalative polymerization. *Polymer* [online]. 2012, **53**(22), 5060–5068 [vid. 2023-05-16]. ISSN 0032-3861. Dostupné z: doi:10.1016/J.POLYMER.2012.09.008

[15] CHO, Tae Woong a Seong Woo KIM. Morphologies and properties of nanocomposite films based on a biodegradable poly(ester)urethane elastomer. *Journal of Applied Polymer Science* [online]. 2011, **121**(3), 1622–1630. ISSN 00218995. Dostupné z: doi:10.1002/app.33766

[16] CHOI, Myung Chan, Ji Yoen JUNG, Hyun Sik YEOM a Young Wook CHANG. Mechanical, thermal, barrier, and rheological properties of poly(ether-block-amide) elastomer/organoclay nanocomposite prepared by melt blending. *Polymer Engineering and Science* [online]. 2013, **53**(5), 982–991. ISSN 00323888. Dostupné z: doi:10.1002/pen.23348

[17] KAZEMI, Amir, Saied NOURI KHORASANI, Mohammad DINARI a Shahla KHALILI. Mechanical and barrier properties of LLDPE/TPS/OMMT packaging film in the presence of POE-g-IA or POE-g-MA. *Journal of Polymer Research* [online]. 2021, **28**(4). ISSN 15728935. Dostupné z: doi:10.1007/s10965-021-02465-6

[18] KATO, Makoto, Arimitsu USUKI, Naoki HASEGAWA, Hirotaka OKAMOTO a Masaya KAWASUMI. Development and applications of polyolefin– and rubber–clay nanocomposites. *Polymer Journal* [online]. 2011, **43**(7), 583–593. ISSN 0032-3896. Dostupné z: doi:10.1038/pj.2011.44

[19] CHOI, Myung Chan, Ji Yoen JUNG, Hyun Sik YEOM a Young Wook CHANG. Mechanical, thermal, barrier, and rheological properties of poly(ether-block-amide) elastomer/organoclay nanocomposite prepared by melt blending. *Polymer Engineering and Science* [online]. 2013, **53**(5), 982–991. ISSN 00323888. Dostupné z: doi:10.1002/pen.23348

[20] KAZEMI, Amir, Saied NOURI KHORASANI, Mohammad DINARI a Shahla KHALILI. Mechanical and barrier properties of LLDPE/TPS/OMMT packaging film in the presence of POE-g-IA or POE-g-MA. *Journal of Polymer Research* [online]. 2021, **28**(4). ISSN 15728935. Dostupné z: doi:10.1007/s10965-021-02465-6

[21] HA, Heonjoo, Jaesung PARK, Ki Ryong HA, Benny D. FREEMAN a Christopher J. ELLISON. Synthesis and gas permeability of highly elastic poly(dimethylsiloxane)/graphene oxide composite elastomers using telechelic polymers. *Polymer* [online]. 2016, **93**, 53–60. ISSN 00323861. Dostupné z: doi:10.1016/j.polymer.2016.04.016

[22] HOFMANN, Daniel, Ralf THOMANN a Rolf MÜLHAUPT. Thermoplastic SEBS Elastomer Nanocomposites Reinforced with Functionalized Graphene Dispersions. *Macromolecular Materials and Engineering* [online]. 2018, **303**(1). ISSN 14392054. Dostupné z: doi:10.1002/mame.201700324

[23] WU, Yun hui, Yong LIN, Yong WEI, Song CHEN, Shu qi LIU a Lan LIU. Constructing interconnected graphene network in fluoroelastomer composites by F-H polar interaction for enhanced mechanical and barrier properties. *Composites Science and Technology* [online]. 2017, **148**, 35–42. ISSN 02663538. Dostupné z: doi:10.1016/j.compscitech.2017.05.014

[24] KANG, Hailan, Kanghua ZUO, Zhao WANG, Liqun ZHANG, Li LIU a Baochun GUO. Using a green method to develop graphene oxide/elastomers

nanocomposites with combination of high barrier and mechanical performance. *Composites Science and Technology* [online]. 2014, **92**, 1–8. ISSN 02663538. Dostupné z: doi:10.1016/j.compscitech.2013.12.004

[25] SADASIVUNI, Kishor Kumar, Allisson SAITER, Nicolas GAUTIER, Sabu THOMAS a Yves GROHENS. Effect of molecular interactions on the performance of poly(isobutylene-co- isoprene)/graphene and clay nanocomposites. *Colloid and Polymer Science* [online]. 2013, **291**(7), 1729–1740. ISSN 0303402X. Dostupné z: doi:10.1007/s00396-013-2908-y

[26] SANGRONIZ, Ainara, Leire SANGRONIZ, Alba GONZALEZ, Antxon SANTAMARIA, Javier DEL RIO, Marian IRIARTE a Agustin ETXEBERRIA. Improving the barrier properties of a biodegradable polyester for packaging applications. *European Polymer Journal* [online]. 2019, **115**, 76–85. ISSN 00143057. Dostupné z: doi:10.1016/j.eurpolymj.2019.03.026

[27] SRIVASTAVA, Aviral a Sumit SHARMA. Recent advances in experimental and molecular dynamics study of graphene-oxide/natural rubber composites: A review. *Journal of Reinforced Plastics and Composites* [online]. 2023, **42**(3–4), 110–130. ISSN 0731-6844. Dostupné z: doi:10.1177/07316844221102939

[28] PADUVILAN, Jibin Keloth, Prajitha VELAYUDHAN, Ashin AMANULLA, Hanna Joseph MARIA, Allisson SAITER-FOURCIN a Sabu THOMAS. Assessment of graphene oxide and nanoclay based hybrid filler in chlorobutyl-natural rubber blend for advanced gas barrier applications. *Nanomaterials* [online]. 2021, **11**(5). ISSN 20794991. Dostupné z: doi:10.3390/nano11051098

[29] ZHANG, Jianfeng, Shuai LIANG, Liyun YU, Anne LADEGAARD SKOV, Hussein M. ETMIMI, Peter E. MALLON, Alex ADRONOV a Michael A. BROOK. Silicone-modified graphene oxide fillers via the Piers-Rubinsztajn reaction. *Journal of Polymer Science, Part A: Polymer Chemistry* [online]. 2016, **54**(15), 2379–2385. ISSN 10990518. Dostupné z: doi:10.1002/pola.28112

[30] EVGIN, Tuba, Matej MIČUŠÍK, Peter MACHATA, Hamed PEIDAYESH, Jozef PREŤO a Mária OMASTOVÁ. Morphological, Mechanical and Gas Penetration Properties of Elastomer Composites with Hybrid Fillers. *Polymers* [online]. 2022, **14**(19). ISSN 20734360. Dostupné z: doi:10.3390/polym14194043

[31] WU, Yun hui, Yong LIN, Yong WEI, Song CHEN, Shu qi LIU a Lan LIU. Constructing interconnected graphene network in fluoroelastomer composites by F-H polar interaction for enhanced mechanical and barrier properties. *Composites Science and Technology* [online]. 2017, **148**, 35–42 [vid. 2023-05-16]. ISSN 0266-3538. Dostupné z: doi:10.1016/J.COMPSCITECH.2017.05.014

[32] SADASIVUNI, Kishor Kumar, Allisson SAITER, Nicolas GAUTIER, Sabu THOMAS a Yves GROHENS. Effect of molecular interactions on the performance of poly(isobutylene-co- isoprene)/graphene and clay nanocomposites. *Colloid and Polymer Science* [online]. 2013, **291**(7), 1729–1740. ISSN 0303402X. Dostupné z: doi:10.1007/s00396-013-2908-y

[33] EVGIN, Tuba, Matej MIČUŠÍK, Peter MACHATA, Hamed PEIDAYESH, Jozef PREŤO a Mária OMASTOVÁ. Morphological, Mechanical and Gas Penetration Properties of Elastomer Composites with Hybrid Fillers. *Polymers* [online]. 2022, **14**(19). ISSN 20734360. Dostupné z: doi:10.3390/polym14194043

[34] CADAMBI, R. M. a E. GHASSEMIEH. Hard coatings on elastomers for reduced permeability and increased wear resistance. In: *Plastics, Rubber and Composites* [online]. 2012, s. 169–174. ISSN 14658011. Dostupné z: doi:10.1179/1743289811Y.0000000048

[35] PARAENSE, Mariana Ogando, Thiago Henrique Rodrigues DA CUNHA, Andre Santarosa FERLAUTO a Kátia Cecília DE SOUZA FIGUEIREDO. Monolayer and bilayer graphene on polydimethylsiloxane as a composite membrane for gas-barrier applications. *Journal of Applied Polymer Science* [online]. 2017, **134**(47). ISSN 10974628. Dostupné z: doi:10.1002/app.45521

[36] CHO, Chungyeon, Fangming XIANG, Kevin L. WALLACE a Jaime C. GRUNLAN. Combined Ionic and Hydrogen Bonding in Polymer Multilayer Thin Film for High Gas Barrier and Stretchiness. *Macromolecules* [online]. 2015, **48**(16), 5723–5729. ISSN 15205835. Dostupné z: doi:10.1021/acs.macromol.5b01279

[37] OCHIRKHUYAG, Nyamjargal, Yuuki NISHITAI, Satoru MIZUGUCHI, Yuji ISANO, Sijie NI, Koki MURAKAMI, Masaki SHIMAMURA, Hiroki IIDA, Kazuhide UENO a Hiroki OTA. Stretchable Gas Barrier Films Using Liquid Metal toward a Highly Deformable Battery. *ACS Applied Materials and Interfaces* [online]. 2022, **14**(42), 48123–48132. ISSN 19448252. Dostupné z: doi:10.1021/acsami.2c13023

[38] PRAVEEN, S., P. K. CHATTOPADHYAY, P. ALBERT, V. G. DALVI, B. C. CHAKRABORTY a S. CHATTOPADHYAY. Synergistic effect of carbon black and nanoclay fillers in styrene butadiene rubber matrix: Development of dual structure. *Composites Part A: Applied Science and Manufacturing* [online]. 2009, **40**(3), 309–316. ISSN 1359835X. Dostupné z: doi:10.1016/j.compositesa.2008.12.008

[39] ABULYAZIED, Dalia E. a Antoaneta ENE. *An investigative study on the progress of nanoclay-reinforced polymers: Preparation, properties, and applications: A review* [online]. B.m.: MDPI. 1. prosinec 2021. ISSN 20734360. Dostupné z: doi:10.3390/polym13244401

[40] *https://standards.globalspec.com/std/854271/ds-en-13925-1*.

[41] SHRIVASTAVA, Anshuman. Plastic Properties and Testing. *Introduction to Plastics Engineering* [online]. 2018, 49–110 [vid. 2023-05-08]. Dostupné z: doi:10.1016/B978-0-323-39500-7.00003-4

[42] ANTON PAAR GMBH. *https://wiki.anton-paar.com/en/basics-of-rheology/rheological-measurements/*.

[43] *https://standards.globalspec.com/std/9958505/iso-6721-10*.

[44] KAROUI, Romdhane. DSC Analysis. *Chemical Analysis of Food: Techniques and Applications*. 2012, 499–517.

[45] ALMOSELHY, Rania I M. *Applications of Differential Scanning Calorimetry (DSC) in Oils and Fats Research. A Review* [online]. nedatováno. Dostupné z: www.arjonline.org

[46] *https://standards.globalspec.com/std/3848990/astm-e537-12*.

[47] *https://standards.globalspec.com/std/3833778/ASTM%20E1356-08*.

[48] *https://standards.globalspec.com/std/14477031/astm-e2425-21*.

[49] *https://standards.globalspec.com/std/13326731/iso-6721-11*.

[50] SONGHAN, Contact. *Modifier Concentration, meq/ 100g clay 125 Organic Modifier dimethyl, dihydrogenated tallow, quaternary ammonium X-Ray Diffraction d-Spacing (001) 31.5 Angstroms Descriptive Properties Value Comments* [online]. nedatováno. Dostupné z: www.lookpolymers.com

[51] SONGHAN, Contact. *Modifier Concentration, meq/ 100g clay 90 Organic Modifier methyl, tallow, bis-2-hydroxyethyl, quaternary ammonium X-Ray Diffraction d-Spacing (001) 18.5 Angstroms Descriptive Properties Value Comments* [online]. nedatováno. Dostupné z: www.lookpolymers.com

LIST OF ABBREVIATIONS

TPE Thermoplastic elastomers

TPU Thermoplastic polyurethane

GO Graphene oxid

TPU TPU 11T80

TPU ECO TPU ECO D12T80E

GO 1 ES 100 C10

GO 2 ES 500 F5

MMT Montmorillonite

MMT 15 A Cloisite 15A

MMT 30 B Cloisite 30B

DSC Differencial Scanning Calorimetry

DMA Dynamic Mechanical Analysis

XRD/WAXD X-Ray Diffraction/Wide-Angle X-Ray Diffraction

LIST OF FIGURES

Figure 1: Compounding machine. 26

Figure 2: Granulation machine 26

Figure 3: Detail of granulating head 27

Figure 4: Extrusion conditions of TPU 11T80 with MMT fillers 27

Figure 5: Extrusion conditions of TPU 11T80 with GO 2 filler 28

Figure 6: BOCOMATIC EB 25 machine 29

Figure 7: Photo of poor GO 2 filler dispersion in TPU matrix (left picture) 29

Figure 8: Photo of good MMT filler dispersion in TPU matrix (right picture) 29

Figure 9: Anton Paar, XRDynamic 500 30

Figure 10: XRD measurement record for pure TPU 11T80, the vertical axis plots the intensity [cts.] and the x-axis plots the angle values 2Θ [°]. The yellow curve shows the course of the measurement itself, the other curves are the result of peaks fitting and backgrounds, and the pink curve shows proportion of amorphous phase. 31

Figure 11: XRD measurement record for pure TPU ECO D12T80E 11T80, the vertical axis plots the intensity [cts.] and the x-axis plots the angle values 2Θ [°]. The yellow curve shows the course of the measurement itself, the other curves are the result of peaks fitting and background, and the pink curve shows proportion of amorphous phase. 32

Figure 12: XRD measurement record for MMT 15 A powder, the vertical axis plots the intensity [cts.] and the x-axis plots the angle values 2Θ [°]. The yellow curve shows the course of the measurement itself, the other curves are the result of peaks fitting and background, and the pink curve shows proportion of amorphous phase. 33

Figure 13: XRD measurement record for MMT 15 A + TPU masterbatch, the vertical axis plots the intensity [cts.] and the x-axis plots the angle values 2Θ [°]. The yellow curve shows the course of the measurement itself, the other curves are the result of peaks fitting and background, and the pink curve shows proportion of amorphous phase. 33

Figure 14: XRD measurement record for MMT 30 B powder, the vertical axis plots the intensity [cts.] and the x-axis plots the angle values 2Θ [°]. The yellow curve shows the course of the measurement itself, the other curves are the result of peaks fitting and background, and the pink curve shows proportion of amorphous phase. 34

Figure 15: XRD measurement record for MMT 30 B + TPU masterbatch, the vertical axis plots the intensity [cts.] and the x-axis plots the angle values 2Θ [°]. The yellow curve shows the course of the measurement itself, the other curves are the result of peaks fitting and background and the pink curve shows proportion of amorphous phase. 35

Figure 16: XRD measurement record for GO 2 powder, the vertical axis plots the intensity [cts.] and the x-axis plots the angle values 2Θ [°]. The yellow curve shows the course of the measurement itself, the other curves are the result of peaks fitting and background the pink curve shows proportion of amorphous phase. 36

Figure 17: XRD measurement record for MMT 30 B + TPU masterbatch, the vertical axis plots the intensity [cts.] and the x-axis plots the angle values 2Θ [°]. The yellow curve shows the course of the measurement itself, the other curves are the result of peaks fitting and background, and the pink curve shows proportion of amorphous phase. 36

Figure 18: Anton Paar's Modular Compact Rheometer MCR 502 38

Figure 19: Dependence of Storage Modulus G´ [Pa] on frequency change [rad/s] for pure TPUs and TPU 11T80 nanocomposites with MMT fillers 15 A (20 wt.%) and 30 B (20 wt.%) and GO2 (10 wt.%). 39

Figure 20: Dependence of Loss Factor tanδ on frequency change [rad/s] for pure TPUs and TPU 11T80 nanocomposites with MMT fillers 15 A (20 wt.%) and 30 B (20 wt.%) and GO2 (10 wt.%). 40

Figure 21: Dependence of Complex Viscosity [Pa.s] on frequency change [rad/s] for pure TPUs and TPU 11T80 nanocomposites with MMT fillers 15 A (20 wt.%) and 30 B (20 wt.%), and GO2 (10 wt.%); the sample was tested immediately after pressing.. 41

Figure 22: Dependence of Complex viscosity [Pa.s] on frequency change [rad/s] for pure TPUs and TPU 11T80 nanocomposites with MMT fillers 15 A (20 wt.%) and 30 B (20 wt.%), and GO2 (10 wt.%), this measurement was made on the same specimen as the previous one, but meanwhile it was cooled and reheated and went through deformation. . 41

Figure 23: Dependence of Complex Shear Modulus G* [Pa] on temperature [°C] for pure TPUs and TPU 11T80 nanocomposites with MMT fillers 15 A (20 wt.%) and 30 B (20 wt.%) and GO2 (10 wt.%). (Cooling 190-80°C) 42

Figure 24: Dependence of Complex Shear Modulus G* [Pa] on temperature [°C] for pure TPUs and TPU 11T80 nanocomposites with MMT fillers 15 A (20 wt.%) and 30 B (20 wt.%) and GO2 (10 wt.%). (Heating 80-190°C) 43

Figure 25:Dependence of Loss Factor tanδ on temperature [°C] for pure TPUs and TPU 11T80 nanocomposites with MMT fillers 15 A (20 wt.%) and 30 B (20 wt.%) and GO2 (10 wt.%). (Cooling 190-80 °C) 44

Figure 26: Dependence of Loss Factor tanδ on temperature [°C] for pure TPUs and TPU 11T80 nanocomposites with MMT fillers 15 A (20 wt.%) and 30 B (20 wt.%) and GO2 (10 wt.%). (Heating 80-190 °C) 45

Figure 27: DSC 1 by Mettler Toledo 46

Figure 28: DSC measurement record for pure TPU 11T80 47

Figure 29: DSC measurement record for pure TPU ECO D12T80E 48

Figure 30: DSC measurement record for MMT 15 A 49

Figure 31: DSC measurement record for MMT 30 B 50

Figure 32: DSC measurement record for GO2 51

Figure 33: DMA 1 by Mettler Toledo 52

Figure 34: DMA results for all materials, top graph: dependence of E´ modulus on temperature, bottom graph: dependence of tanδ on temperature 53

Figure 35: VAC - V1 Labthink® 54

Figure 36: Average GTR values [cm^3/m^2.day.0.1MPa] for pure TPU and TPU nanocomposites with MMT fillers 15 A (5 wt.%) and 30 B (5 and 10 wt.%) 55

Figure 37: Average of permeability parametr *P* values [Barrer] for pure TPU and TPU nanocomposites with MMT fillers 15 A (5 wt.%) and 30 B (5 and 10 wt.%) 55

LIST OF TABLES

Table 1: Percentage of crystalline and amorphous phase of TPU 11T80 31
Table 2:Percentage of crystalline and amorphous phase of TPU ECO D12T80E 32
Table 3: Percentage of crystalline and amorphous phase of MMT 15 A powder 33
Table 4: Percentage of crystalline and amorphous phase of MMT 15 A + TPU masterbatch 34
Table 5: Percentage of crystalline and amorphous phase of MMT 30 B powder 34
Table 6: Percentage of crystalline and amorphous phase of MMT 30 B + TPU masterbatch 35
Table 7: Percentage of crystalline and amorphous phase of GO 2 powder 36
Table 8: Percentage of crystalline and amorphous phase of GO 2+ TPU masterbatch 37
Table 9: Measured and average values of the GTR parameter 54
Table 10: Measured and average values of the permeability parametr *P* 55